International Journal of Engineering and Geosciences
https://dergipark.org.tr/en/pub/ijeg
e-ISSN 2548-0960



Sentinel-5P TROPOMI Data-Based Spatiotemporal Variations and Trends of Atmospheric Gaseous Pollutants in Dinajpur District, Bangladesh

Md. Mahfuj Ahmed Sizan [1], Md. Mahabub Rahman [*], Md. Osman Gani Rasel [1], Mehedy Sultan Sohan [1], Pallab Nag [1]

[1] Hajee Mohammad Danesh Science and Technology University, Dept. of Civil Engineering, Bangladesh, mdmahfuj.sizan@gmail.com, mmr.civil@hstu.ac.bd, raselosman25@gmail.com, sultansohan2016@gmail.com, pallabnag001@gmail.com

Cite this study: Sizan, M.M.A., Rahman, M.M., Rasel, M.O.G., Sohan, M.S., & Nag, P. (2026). Sentinel-5P TROPOMI Data-Based Spatiotemporal Variations and Trends of Atmospheric Gaseous Pollutants in Dinajpur District, Bangladesh. International Journal of Engineering and Geosciences, 11 (3), 701-721.

https://doi.org/10.26833/ijeg.1841881

Keywords
Air Quality
Sentinel-5P
Nitrogen Dioxide
Ozone
Carbon Monoxide

Research Article

Received: 14.12.2025
Revised: 16.03.26
Accepted: 22.04.26
Published:01.10.2026



Abstract

Air pollution is now a major environmental and public health problem in many parts of South Asia, but it remains under-monitored at ground level. Utilizing the Google Earth Engine, the present study analyzes the spatiotemporal pattern of five major atmospheric pollutants (NO_2, SO_2, CO, O_3, and HCHO) over Dinajpur District in northern Bangladesh from space-borne observations with the Sentinel-5P Tropospheric Monitoring Instrument (TROPOMI). Multi-temporal datasets spanning 2019–2023 were employed to characterize annual trends, seasonality, and spatial pollution hotspots. Results show a statistically significant upward trend for NO_2 and HCHO ($p < 0.05$), with overall increases of percentage rates of 10.58% and 18.09%, respectively. Annual mean HCHO increased from 0.00019 mol m^{-2} (2019) to 0.00023 mol m^{-2} (2023), and peak NO_2 levels were 0.00010 mol m^{-2} in 2023. SO_2 showed an upward trend in background concentration, with the annual mean of 0.00043 mol m^{-2} in 2023, while CO showed a more stable trend, with a maximum value of its peak mean being 0.0438 mol m^{-2} (in 2021). The accumulation of O_3 on the tree crowns steadily increased from 0.119 mol m^{-2} (2019) to 0.126 mol m^{-2} (2022) and then slightly decreased in 2023. The spatial analysis revealed long-lasting multi-pollutant hotspots associated with brick kilns, transportation activity, and expanding urbanization in the central-western urban corridor of Dinajpur. The Integrated Air Quality Risk Index shows the risk concentration in air quality around Dinajpur Sadar and near industrial areas. Such findings highlight the ability of satellite-based observations to capture pollution dynamics and deliver essential evidence for regional air-quality management and environmental policy development in data-scarce regions.

1. Introduction

Air pollution persistently ranks among the most concerning environmental and public health problems worldwide, particularly in developing countries undergoing rapid economic growth, population increase, and urbanization that mostly correlated with augmented emissions from anthropogenic and natural sources. Various kinds of pollutants in the atmosphere, including nitrogen dioxide (NO_2), sulfur dioxide (SO_2), carbon monoxide (CO), ozone (O_3) as well as formaldehyde (HCHO), are significantly affecting human health, climate system and ecological balance [1-2]. Multiple epidemiological investigations have found that long-term exposure to such pollution sources is linked with an elevated risk of cardiovascular diseases, respiratory infections, chronic obstructive pulmonary disease (COPD), lung cancer and premature death [3-4]. Also, air pollution leads to decreased agricultural productivity, inferior visibility, acid deposition and change in regional atmosphere chemistry [5-6].

South Asia is recognized as one of the severely polluted regions of the world and is home to some of the fastest growing economies (India, Pakistan, Bangladesh), which have been experiencing unprecedented increases in airway pollution [7-8]. Especially, Bangladesh reportedly consistently remains one of the top-ranked nations to possess highest pollutant load in the atmosphere due to poor emission controls, unbound industrialization, rampant fossil fuel consumption and large-scale biomass burning [9]. Although air quality research has primarily focused on metropolitan areas

like Dhaka [10], Chittagong [11], Rajshahi [12] and Gazipur [13], smaller urban/semiurban districts to which Dinajpur in the north of Bangladesh belongs are receiving less attention despite experiencing increasing environmental pressures due to new urbanization, intensifying agricultural practices, and industrial growth.

There are noticeable recent years' trends in socio-economic developments of Dinajpur District, such as a boom in the number of brick kilns, an upsurge of rice mills and agro-industries, intensification of vehicle movements, and transformation of rural into urban areas [14]. These activities are identified as sources of NO_2, SO_2, CO, O_3 precursors, and HCHO that collectively affect the local and regional air quality. For instance, brick kilns are the largest stationary sources of NO_x and SO_2 in Bangladesh as a result of the burning of high-sulfur coal and firewood [15]. Vehicular emissions play a similar role in the enhancement of CO and NO_2, especially in sites where waste burning is more common and hence, contributes to higher levels of CO and HCHO [16-17]. Biomass burning due to poor combustion efficiencies, biofuel use for cooking, combined with agro-residual burning, results in significant levels of HCHO. Ozone, which is a secondary pollutant, is produced by intricate photochemical reactions of nitrogen oxides and volatile organic compounds (VOCs), under the influence of solar radiation, such as having high sensitivity to precursor emissions and meteorological conditions [18-19].

Reliable monitoring of air quality is necessary to gain insight into pollution mechanisms and support effective governmental policies on the environment. But Bangladesh has no substantial system to measure air quality at the ground, much less in a district like Dinajpur, where there are no continuous measurement facilities. This limitation has led to an urgent requirement for complementary monitoring modes that can offer reliable, spatially consistent, long-term atmospheric data. In this regard, satellite remote sensing is becoming a useful approach to estimate air quality over large spatial regions [20-21]. Down to daily temporal resolution, satellite sounders like the Sentinel-5 Precursor (Sentinel-5P) equipped with the Tropospheric Monitoring Instrument (TROPOMI) provide high spatial coverage of tropospheric trace gas measurements over a broad density range and even in data-limited regions, which is already possible [22-23]. Sentinel-5P TROPOMI has also been heavily used in international [24-26] and local context to monitor the tropospheric column densities of NO_2 [27], SO_2 [28-29], O_3 [30], and CO [31-32] and HCHO [33]. Its high temporal frequency and spatial resolution render it especially well-suited to probing pollution trends, pointing out emission hotspots or seasonal changes. With the help of Google Earth Engine (GEE), a cloud-based platform that stores geospatial datasets and provides user-friendly, large-scale processing capabilities, Sentinel-5P is efficiently utilized in retrieving column density values at regional spatial resolutions from multi-temporal datasets [34]. GEE and GIS were effectively utilized by many researchers in the field of civil engineering for various purposes, like forest cover change [35], soil liquefaction prediction [36-38], groundwater depth and quality assessment [39-40], risk assessment [41], seismic microzonation [42-43], N-value correction [44], LULC change detection [45], and bearing capacity evaluation [46].

Recent studies have highlighted the significance of satellite remote sensing and cloud-based geospatial platforms in spatiotemporal analysis for large-scale environmental monitoring. Researchers having access to multi-temporal satellite datasets benefit from platforms such as Google Earth Engine to process large amounts of data and gain the ability to analyze spatial distribution and temporal trends across vast homogeneous geographical areas. Spatiotemporal approaches applied using remote sensing data have been successfully employed to study environmental change and natural hazards [47-48] since that time. These studies illustrate the utility of integrating multi-temporal satellite observations into geospatial analysis frameworks to detect long-term environmental trends and spatial variability, thus supporting the methodological approach undertaken in the current study. Despite such opportunities of advanced remote sensing, an overview of gaseous pollutants in Northern Bangladesh is still scanty. The majority of previous studies have addressed particulate matters, or major urban cities, and large geographical knowledge gaps remain for areas in transformation. As the industrial sector has boomed along with the transportation network and altered land-use in Dinajpur, examining long-term trends on air quality is crucial to observe the potential health risks. Hence, the present study is aimed at offering a detailed spatiotemporal analysis of column densities of NO_2, SO_2, CO, O_3, and HCHO in Dinajpur District over 2019–2023 based on TROPOMI (Sentinel-5P) data retrieved from Google Earth Engine. To address this, here we sought to present an all-round view of the air quality dynamics in Dinajpur by developing annual and monthly distributions, tracing hotspots and analyzing long term trends. The results also add value to the general scientific knowledge bank on regional air quality in South Asia, and are evidence-based input for policy makers, environmental managers and researchers working towards controlling pollution and achieving sustainable development in Bangladesh.

2. Materials and Methods

2.1. Study area

Dinajpur District is situated in the northwestern side of Bangladesh and positioned at 25.6279°N, 88.6332°E. Occupying an area of around 3,400 km^2, the district features a hot semi-arid climate with extremely hot summers and cool to mild winters. The district of Dinajpur is a leading agriculturally productive area and significantly economically important areas in northern Bangladesh, but its land use, population density and industrialization have changed markedly over the last decade. The position of Dinajpur District is depicted in Figure 1 showing various pollutant sources. Brick kilns, rice mills, small and medium industries and the transport sector in the district area too have been adding to more atmospheric pollution. Unprecedented urban development,

enlargement of road coverage and persistent use of biomass and fossil fuels have increased environmental pressures with the result that air quality monitoring represents an urgent need. But Dinajpur, as is the case with most of Bangladesh's secondary cities and semi-urban districts, does not have dedicated ground-based air quality monitoring stations. Illustration of these constraints emphasizes the need for satellite observations to assess pollutant levels and monitor both the spatial and temporal pattern of smog across the region.

2.2. Data

Multi-temporal satellite-based atmospheric pollutant data acquired from the Sentinel-5P TROPOMI instrument for years 2019–2023 have been applied in this study. Five primary gaseous air pollutants, Nitrogen Dioxide (NO_2), Sulfur Dioxide (SO_2), Carbon Monoxide (CO), Ozone (O_3) and Formaldehyde (HCHO) were chosen as these represent the major indicators of anthropogenic emission presence, combustion intensity, photochemical activity and atmospheric reactivity. All datasets were analyzed at their original grid resolution of 1113.2 m for all pollutants. Dinajpur District administrative boundary was selected to be the spatial mask for pollutant extraction and all further analysis. The Level-3 products provided a consistent spatial grid, streamlined use of statistics, and enhanced inter-comparability among pollutants and years.

The Sentinel-5P TROPOMI products used in this study provide tropospheric column densities of atmospheric pollutants, not ground-level surface concentrations. Column density (mol/m^2), which describes the vertical integral of a pollutant, or pollutants, through an atmospheric column. Consequently, the results presented in this study are satellite-derived atmospheric column densities that infer spatial and temporal variation of air pollutants rather than direct measurements of surface-level air pollution.

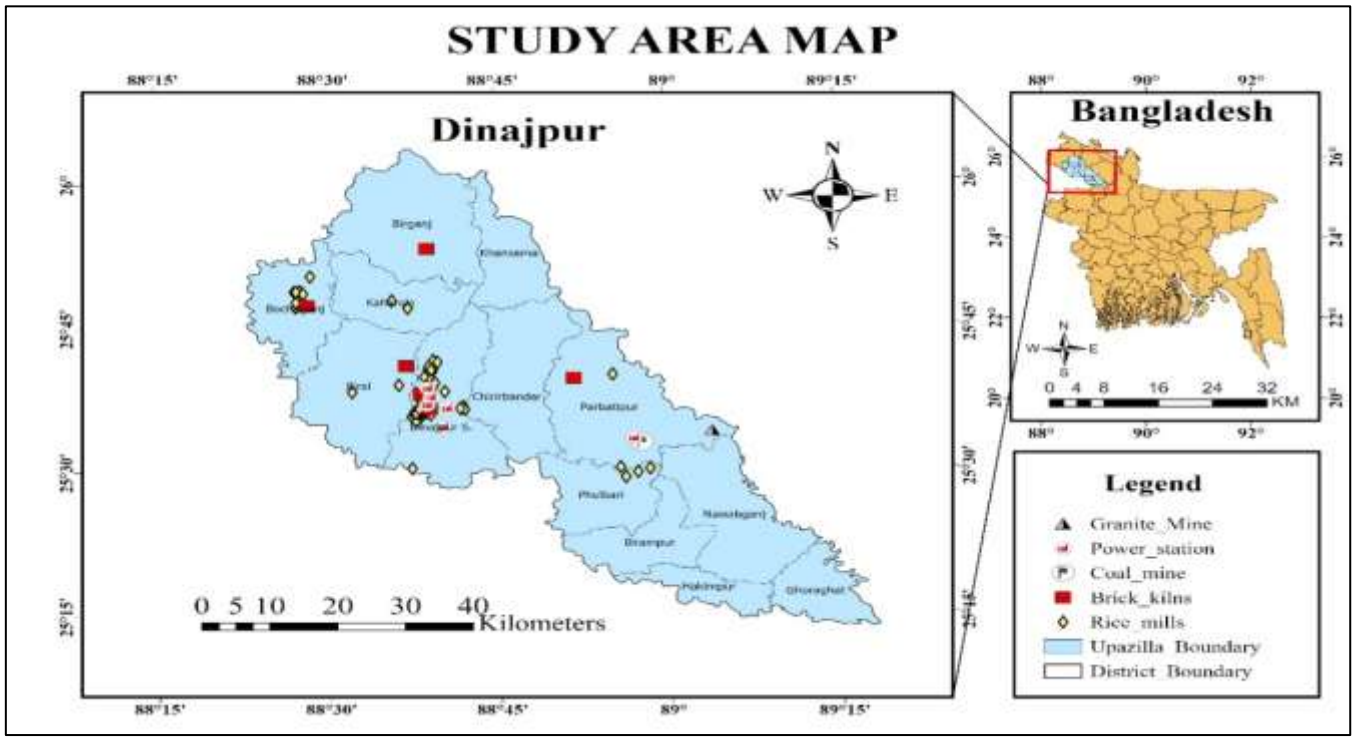


Figure 1. Map of the study region

2.3. Data acquisition and preprocessing in GEE

All the data of pollutants were downloaded, processed and analysed with GEE. We introduced a filter in the COPERNICUS/S5P/OFFL/L3 dataset by pollutant type, and year as for each specific study year (2019-2023). A typical quality assurance filter was used to eliminate retrievals that were cloud contaminated or with low QA values, in order to obtain reliable measurements. The filtered images were clipped to the limits of Dinajpur district boundaries providing spatial homogeneity in these time-series datasets. Composite images were generated for each month by averaging all valid daily scenes during that month. These monthly aggregates were used to study the intra-annual patterns of pollutants and to obtain graphs for their monthly seasonal variation. Composites of yearly mean (2019, 2020, 2021, 2022 and 2023) for each pollutant were derived from monthly means. All monthly data was exported in the form of a CSV file. The Annual composite layers were exported to GeoTIFF (TIF) files for advanced spatial visualization and statistical analysis in ArcGIS Pro. Hence, GEE was adopted for the data retrieval and cloud-free compositing to obtain pollutant surfaces, enabling a homogeneous, reproducible and efficient treatment of the multi-year satellite dataset.

2.4. Data quality and uncertainty

Sentinel 5P TROPOMI reports tropospheric and total column densities of important pollutants (NO_2, SO_2, CO, HCHO, O_3) as vertical column densities instead of surface concentrations, which means the observations reflect the integrated atmospheric burden [sensitive to clouds,

aerosols, and surface albedo through and viewing geometry through the air mass factor calculation] [49-50]. Tropospheric NO_2 columns correlate well with airborne and ground-based DOAS data but typically have a low bias of about 20–40% in polluted areas; this is mainly due to errors in cloud pressure, a priori profiles, and aerosol loading [49, 51]. This is less of a problem for strong (volcanic) and larger anthropogenic plumes, which can be captured at high spatial resolution with TROPOMI SO_2, as individual retrievals near a background level are closer to the detection limit and thus more uncertain, so that SO_2 would not be very reliable when it comes to absolute differences that are small but on average better than detecting large enhancements [52]. For CO, validation against TCCON, NDACC IRWG, and AirCore profiles shows small mean total column biases (a few to 10%) and high correlation but more scatter under cloudy and vertically complex conditions, so the product is most robust for regional plumes rather than precise surface levels [53-54]. FTIR validation globally at 25 sites indicates that HCHO meets its end-user requirement of a 40–80% accuracy range but suffers from concentration-dependent biases and random uncertainty underestimations by about a factor of ~1.6–2.3 times, especially high bias (due to large aerosol loading) in its level at two separate sites in South Asia [50]. For ozone, total column and profile products generally agree with ozonesonde and lidar measurements within ~5–10%, but random uncertainty and some tropospheric underestimations are present at times, as well as an underestimation of ex ante uncertainty estimates at the tropopause [55-56]. The recommended TROPOMI qa_value quality filtering was applied, for each pollutant, to eliminate pixels influenced by clouds, problematic geometry, or retrieval issues, and all fields in this work are considered satellite-derived atmospheric column densities considering the previous uncertainties (i.e., they are reporting relative spatial patterns and temporal trends rather than absolute ground-level concentrations) [49, 54]. HYSPLIT has been shown to acceptably predict for SO_2 and O_3 concentrations less than 10 ppb, and overall, an average of 30–40% of daily observations were filtered out using the recommended QA thresholds outlined for each pollutant dataset. In fact, data loss is more severe during the monsoon seasons, caused by increased coverage of clouds over northern Bangladesh. This eliminates poor measurements and reduces retrieval error, enhancing data reliability but at the expense of temporal coverage during some periods. To avoid possible bias, monthly and annual averages were computed only when enough valid observations were available. Note that as the filtering process was performed in a homogeneous way throughout the entire study period, overall temporal trend analysis is comparable and robust despite limited data availability.

2.5. Data analysis and risk modeling in ArcGIS Pro

The spatial analysis and risk assessment process was conducted in ArcGIS Pro with processed TIF files exported from GEE. Plugin dataset-Each year's pollution layer was visualized with stretched color symbology, and low and high column density subzones were distinctly distinguished. The stretch method retained the full distribution range and demonstrated spatial differences within Dinajpur District. The zonal statistical tools were then used to extract statistical summaries comprising the minimum, maximum, and mean of each year's column densities. Those measures allowed for a quantitative estimate of the interannual variability of pollutants and supported multi-year trend analyses. GEE monthly averages (imported) and annual min–mean–max charts were inserted in the results section to show seasonal and yearly trends.

A multi-criteria decision analysis (MCA) approach was used to generate air pollution risk map, reflecting the total effect of the five selected atmospheric pollutants. For this reason, we recently introduced the air quality risk index (AQRI) to assess the relative spatial distribution of atmospheric pollution risk from satellite-derived column densities. Since different pollutants use different measurement units and magnitudes, we used Min–Max normalization to normalize the values between a range of 0 to 1 according to Equation 1.

$$N_i = \frac{C_i - C_{min}}{C_{max} - C_{min}} \quad (1)$$

where N_i is normalized values and C_i is original column density. In the absence of ground-based exposure measurements and locally validated health-impact coefficients for the study area, equal weighting was used for all pollutants. Similar equal-weight approaches have been adopted in remote sensing–based (environmental) risk assessments where the key goal is relative spatial comparison as opposed to absolute health risk estimation. To reduce the impact of extreme values, normalization limits were based on study-period ranges instead of single-day extremes.

According to Equation 1, we calculated the AQRI 2.

$$AQRI = \frac{1}{n}\sum_{i=1}^{n} N_i \quad (2)$$

where n is the number of pollutants. The AQRI is an indicator of relative spatial pollution risk and does not directly represent exposure to health levels.

The resulting index created an evenly distributed raster of cumulative atmospheric pollution risk, removed the extreme 0.5% outliers due to the percent clip stretch, and then automatically generated labels for the "Low, Medium, and High" points based on the remaining statistical distribution throughout the Dinajpur District. The classification was intended to highlight relative pollution hotspots rather than replicate regulatory air quality standards. This workflow, agglutinating GEE-based preprocessing, statistical analytics at ArcGIS Pro and weighted overlay modeling describes a robust and reproducible method for assessing multi annual trends in pollution and creating spatial risk assessment in areas with no ground monitoring stations. Figure 2 shows the workflow of the study.

2.6 Statistical trend analysis

We used non-parametric statistical methods to quantitatively assess temporal trends of gaseous

atmospheric pollutants, going beyond visual examination. The statistical significance of the monotonic trends in monthly satellite-derived column densities from 2019–2023 was assessed using the Mann–Kendall (MK) trend test. The MK test has been used extensively in environmental time-series analysis because it does not require data to follow a normal distribution and is robust to outliers. Sen's slope estimator is also used to evaluate the value of trends, which determine the median rate of change over time. Statistical significance was assessed at the 95% confidence level ($p < 0.05$). In addition, the percentage change between the first and final observation periods was calculated to give a quantitative estimation of overall trend magnitude (Equation 3).

$$\% \text{ change} = \frac{X_{final} - X_{initial}}{X_{initial}} \times 100 \qquad (3)$$

To explore inter-pollutant relationships and potential common emission sources, correlation analysis among pollutants was performed using Pearson correlation coefficients. All analyses were conducted in R statistical software using the Kendall and trend packages.

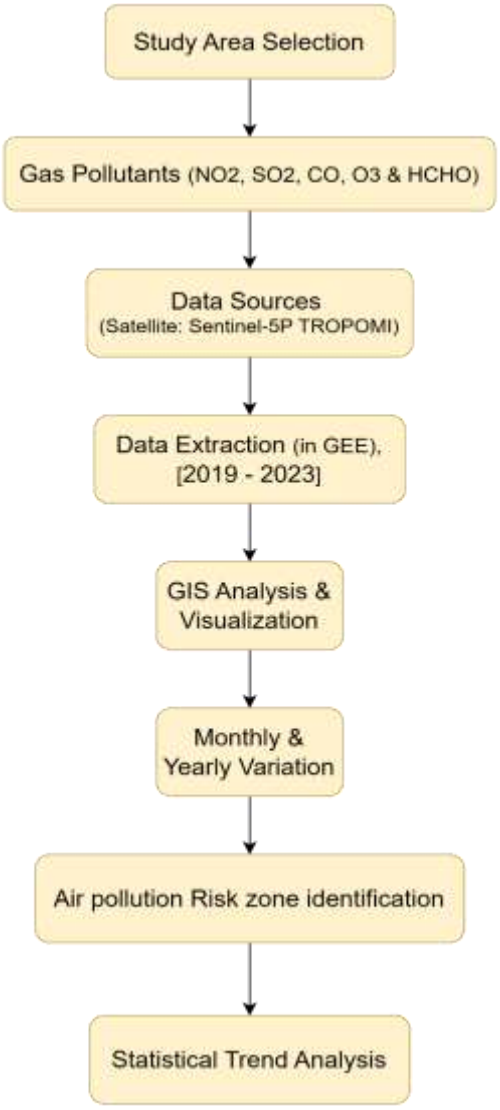


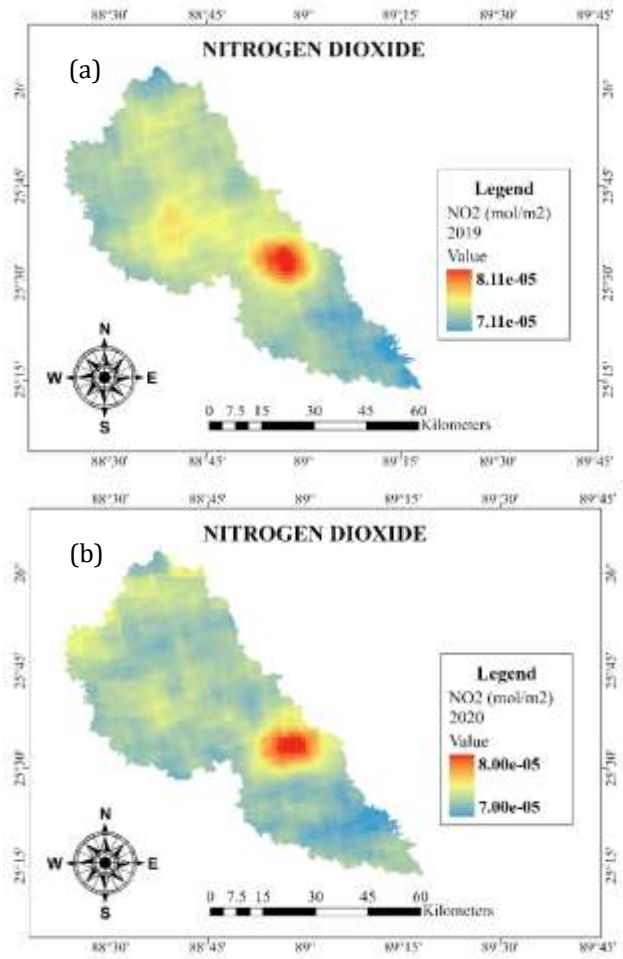
Figure 2. Workflow diagram

3. Results and Discussion

The spatial and temporal variation in five common atmospheric pollutants (NO_2, SO_2, O_3, CO and HCHO) during 2019–2023 were investigated based on the TROPOMI/Sentinel-5P satellite observations, which show significant annual and seasonal dynamics in target area. The annual pollution maps reveal the spatial distribution of each gas, and monthly-average plots as well as annual maximum–minimum–mean plots together outline how concentrations vary within and among years. The outputs are detailed beyond just temporal dynamics, revealing places where the pollutant's intensity is relatively high or low.

3.1. Variation of NO_2

The annual spatial distribution of NO_2 over Dinajpur District is presented in Figures 3(a-e). The maps reveal that the highest column densities of NO_2 were consistent at Dinajpur Sadar, Parbatipur, where a dense transportation network, extended commercial areas, and considerable brick kiln operation exist. These hotspots were consistently present over the five-year period, suggesting long-lasting combustion-emission sources. A seasonal pattern can be found in the examination of monthly averaged vertical column densities (m) of NO_2 over Dinajpur during 2019–2023 (Figures 4a-e). Over the course of the five-year study period, mid-year maxima were consistently found for NO_2 and generally found to fall between April and July.



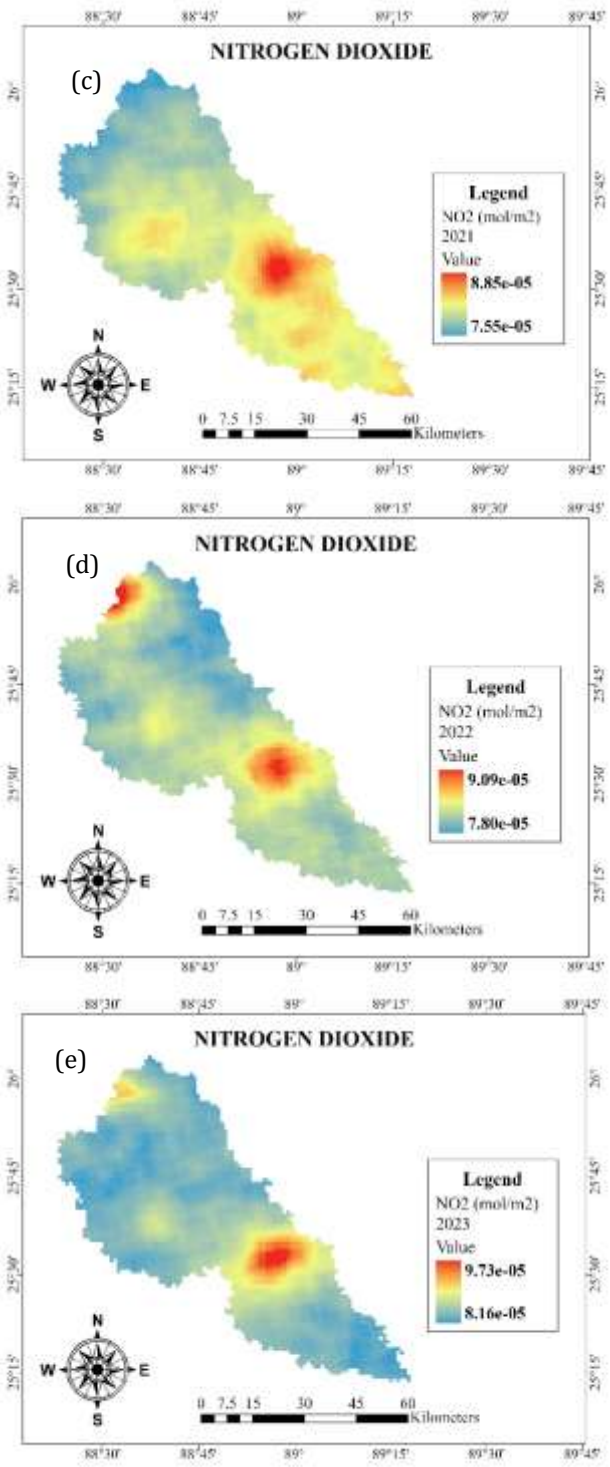
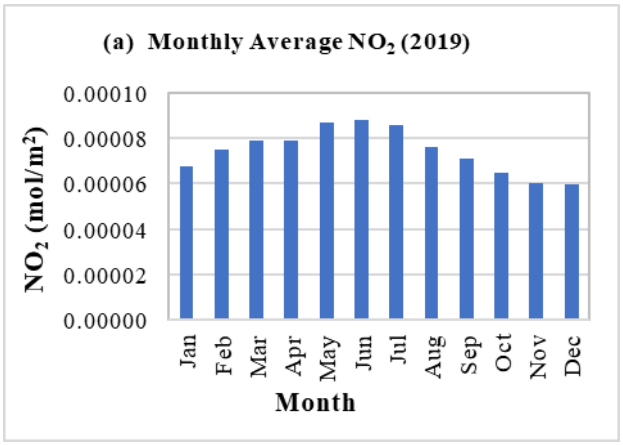
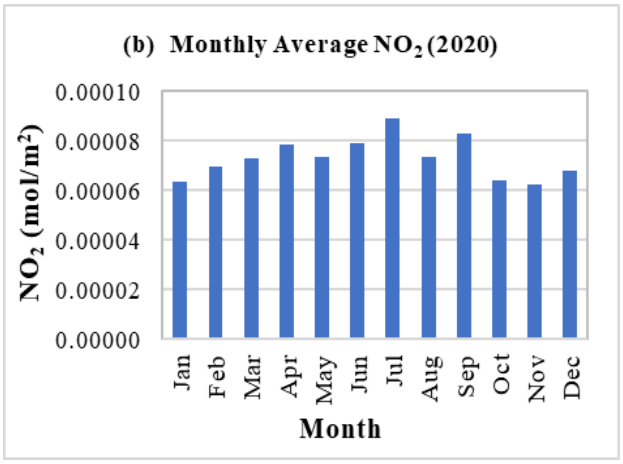
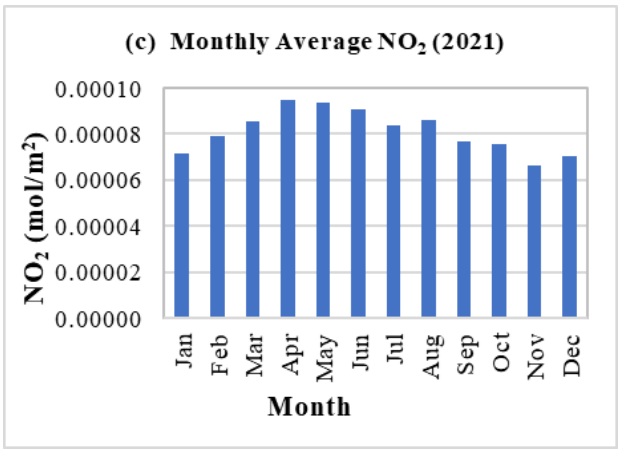


Figure 3. Spatial maps of NO_2 for (a) 2019 (b) 2020 (c) 2021 (d) 2022 (e) 2023

Namely, in 2022 and 2023 the strongest seasonality was observed with peaks in june higher than 0.00010 mol/m². In contrast, the peak magnitude was somewhat lower in 2019 and 2020 (~0.00009 mol/m²). Overall, the data show an accumulation of NO_2 before mid-year and a decrease during late-monsoon to post-monsoon months (August–December). Such cyclic nature indicates that local meteorological state and atmospheric retention of the NO_2 at Dinajpur are strongly interconnected.







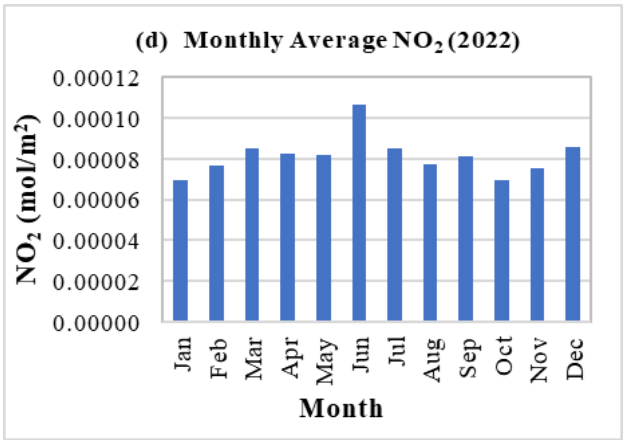




Figure 4. Monthly average values of NO_2 for (a) 2019 (b) 2020 (c) 2021 (d) 2022 (e) 2023

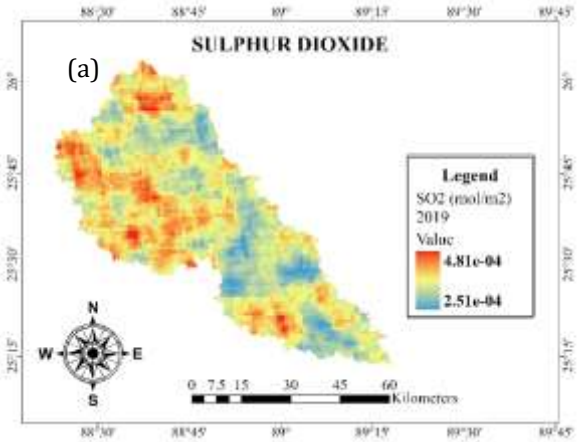
Figure 5 depicts the annual difference in minimum, maximum and mean NO_2 levels. A small drop in 2020 was observed which resulted in the lowest mean and maximum values of the study period. But there is an overall uptick starting in 2021. The greatest pollution occurred during the year 2023 with a maximum value of ~0.00010 mol/m^2 , and the annual mean was higher than in other years.



Figure 5. Comparison of NO_2 based on min-max-mean (2019-2023)

3.2. Variation of SO_2

Annual distribution maps of SO_2 in Figures 6(a-e) show those the highest over Dinajpur Sadar, Biral, Parbatipur and some areas of north-western part of Dinajpur that could be attributed to higher numbers of thick clusters of brick kilns. These hotspots consistently appeared in other years as well, which indicated that kiln activity was closely related to SO_2 emission.



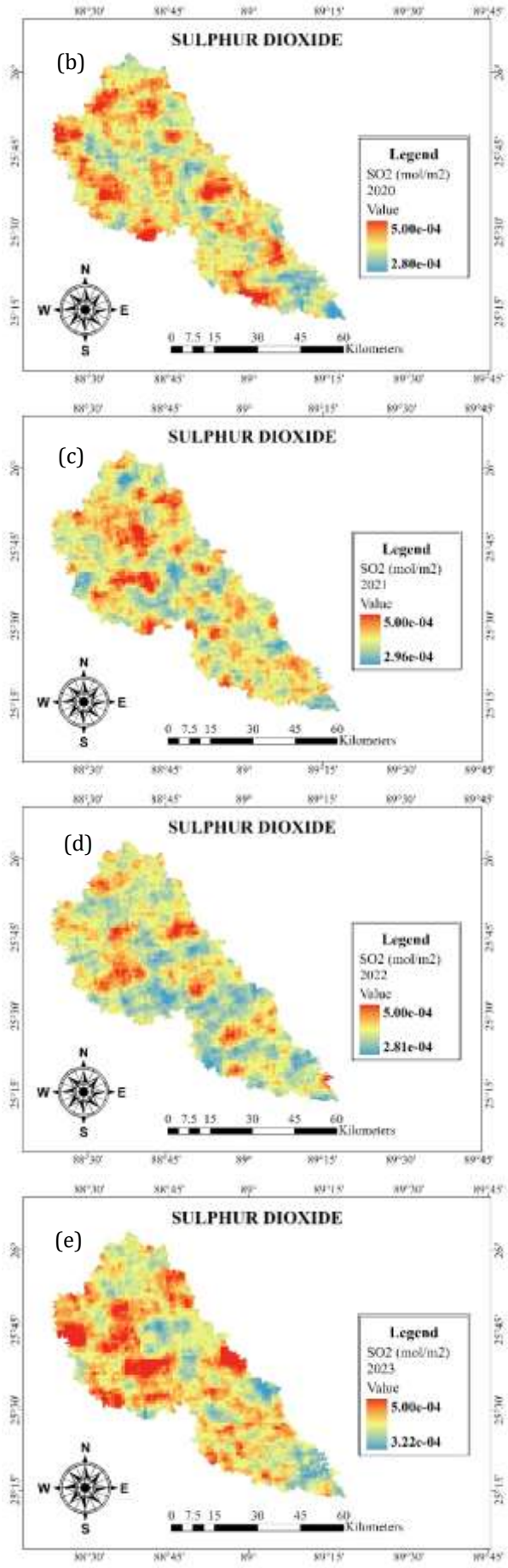
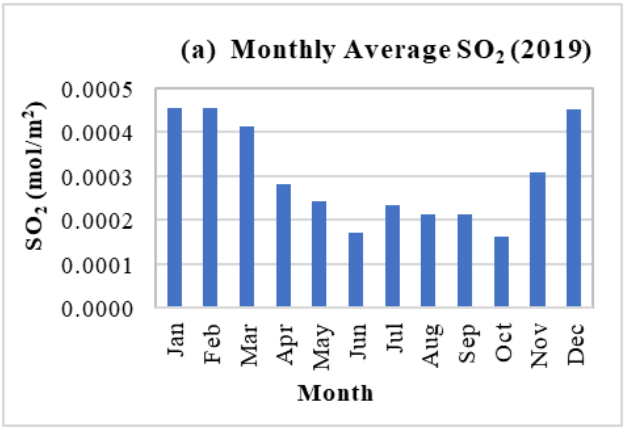
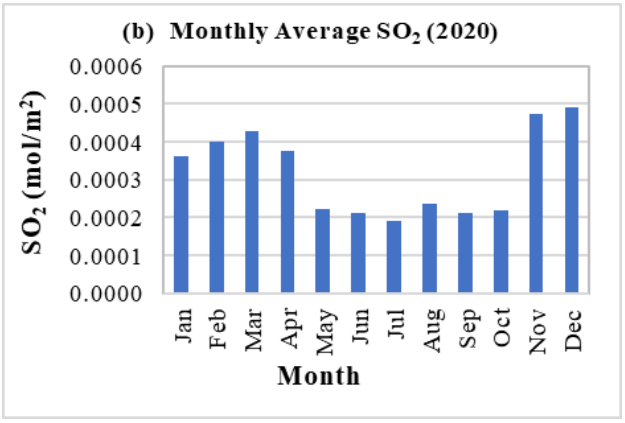
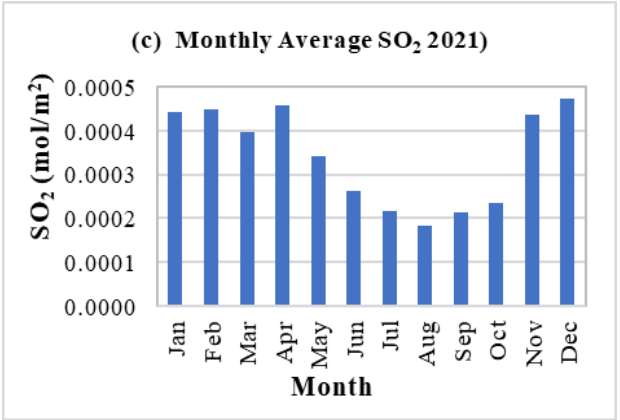


Figure 6. Spatial maps of SO_2 for (a) 2019 (b) 2020 (c) 2021 (d) 2022 (e) 2023

The monthly mean tropospheric column densities of sulfur dioxide over Dinajpur 2019-2023 in Figures 7(a-e) show that there is a similar persistent recurring seasonal behavior through significant occasions in winter accumulation and monsoon dispersal. For all five years, the column densities exhibited a clear U-shape distribution and consistently peaked during the dry winter (January-February) months, typically near 0.0005 mol/m^2. In sharp contrast, the monsoon season (June–October) experienced a drastic removal of pollutants with column densities often less than 0.0002 mol/m^2 by atmospheric washout. Although the overall seasonal trend was strong, local inter-annual variability was seen, including a marked spring pulse in April 2021 and an unprecedented five-month period of persistently low column densities during 2022. Through 2023, the evidence has only bolstered this cycle in place with an end near year-end line-up that staying true to historical trends over the last four years.







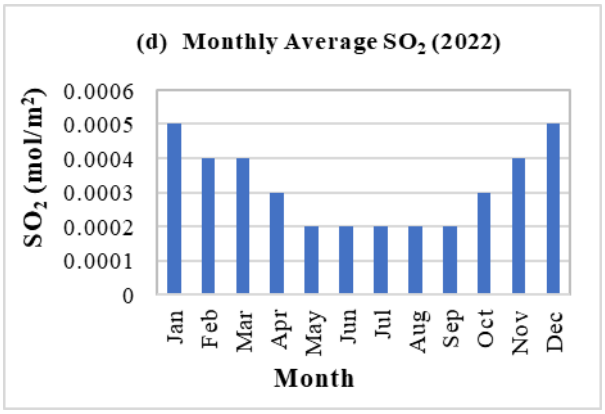




Figure 7. Monthly average values of SO_2 for (a) 2019 (b) 2020 (c) 2021 (d) 2022 (e) 2023

The comparison of the annual SO_2 statistics for Dinajpur (2019–2023) suggests that peak stability and spread in increasing baseline pollution may be divergent (Figure 8).

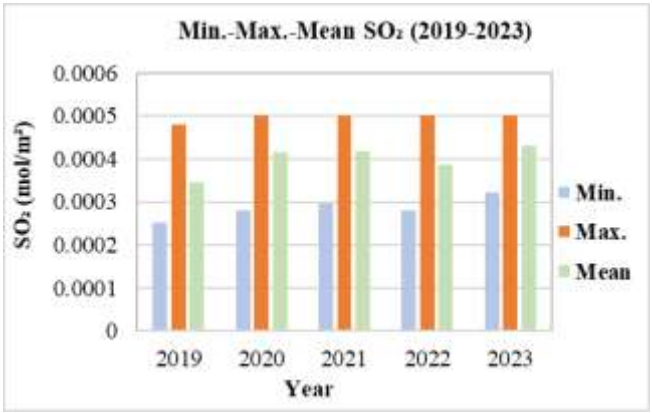
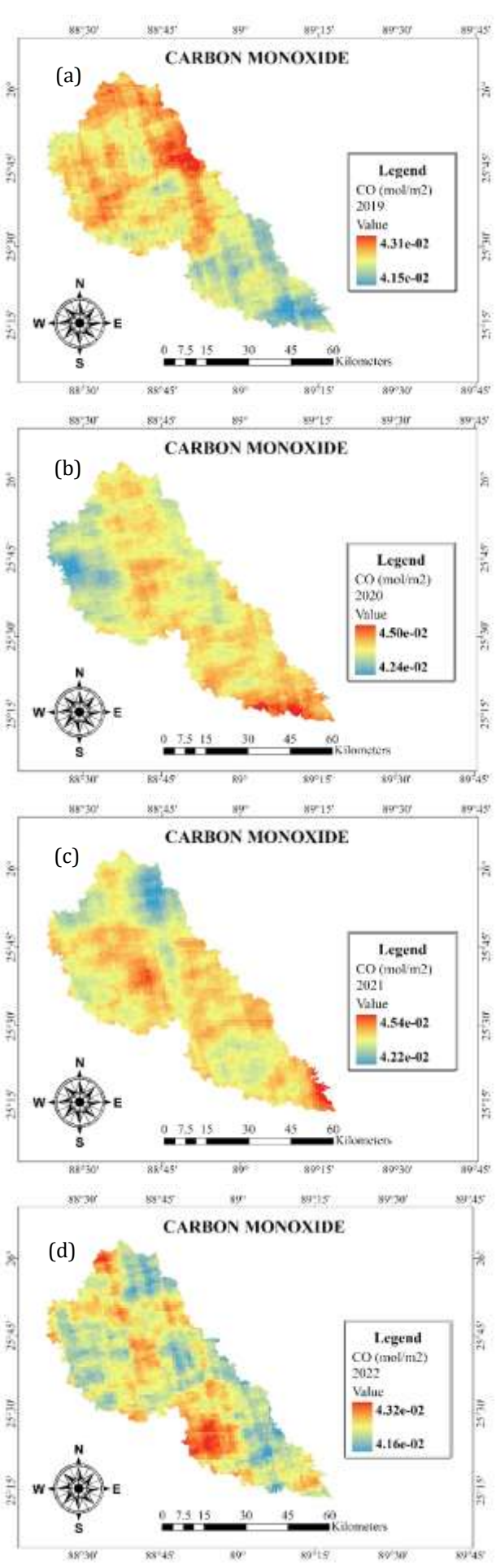


Figure 8. Min-max-mean SO_2 chart (2019-2023)

Although maxima have reached a limit and remained at an almost constant level of about 0.0005 mol/m^2 since 2020, minima exhibit a clear trend upwards namely, from below 0.00025 mol/m^2 in 2019 to more than 0.00032 in the year 2023. The increase in background pollution pushed the annual mean to a new maximum (~0.00043 mol/m^2) in 2023, suggesting that while peak emissions remained unchanged, there is an increasing overall atmospheric SO_2 burden through the year.

3.3. Variation of CO

The spatial patterns of CO for 2019-2023 are presented in Figures 9(a-e).



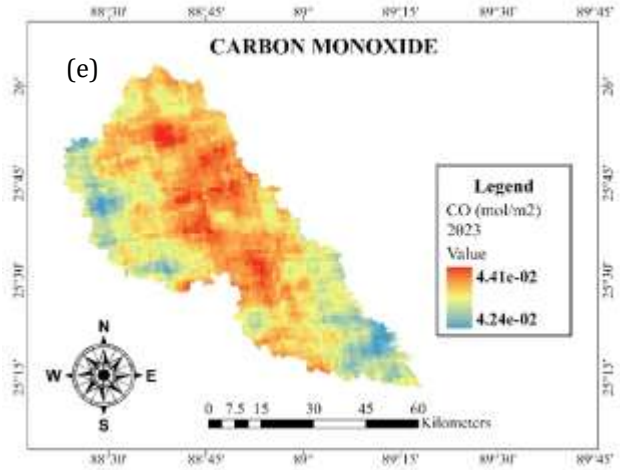
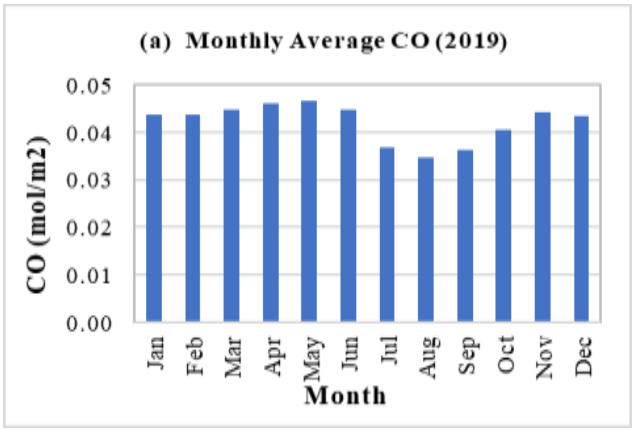
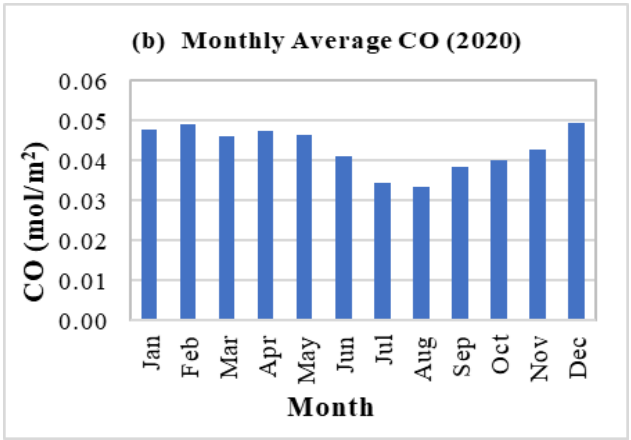
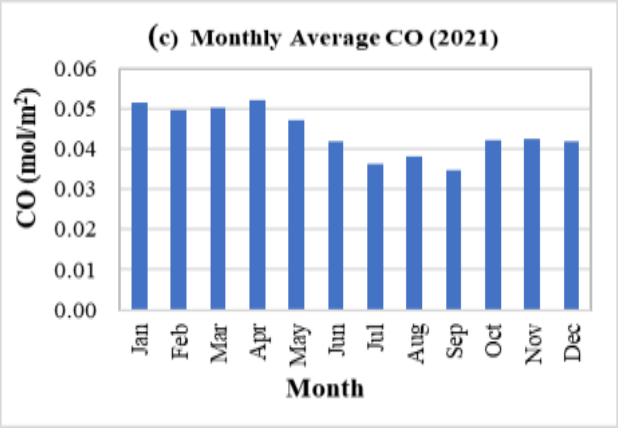


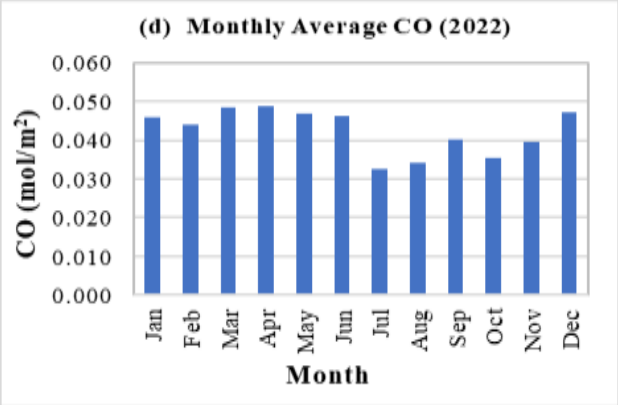
Figure 9. Spatial maps of CO for (a) 2019 (b) 2020 (c) 2021 (d) 2022 (e) 2023

CO was more evenly distributed over the district with some elevation seen near major transport roadways and within urbanized areas like Dinajpur Sadar, Khansama and Phulbari. A strong seasonal cycle of extended dry-season accumulation and monsoon washout characterizes the monthly average CO profile for Dinajpur (2019–2023) (Figures 10a-e). High tropospheric column densities are prevalent from January to May, and maximum values range between 0.047 at 0.052 mol/m^2 (in April 2021). By contrast, the wet season (July–September) is very good in terms of scrubbing the atmosphere, bringing values down to a background of 0.032 mol/m^2 (July 2022) to 0.035 mol/m^2.









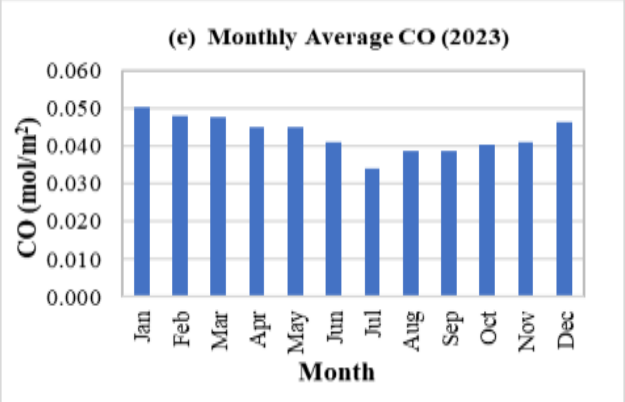


Figure 10. Monthly average values of CO for (a) 2019 (b) 2020 (c) 2021 (d) 2022 (e) 2023

This gradient was best observed in 2023, where across the year CO decreased as a continuous progression from 0.050 mol/m^2 in January to low of 0.034 mol/m^2 in July. The five-year annual statistical observation of carbon monoxide (CO) in Dinajpur skyline offers a different peak of pollution loading on 2021 (Figure 11). The baseline (minimum) column densities remained quite steady at ~0.042 mol/m^2 throughout the period whereas maximum and mean concentration underwent substantial oscillations. The year 2021 registered the largest values among all years (up to 0.0454 mol/m^2, on average 0.0438 mol/m^2). After a slight improvement of the air quality in 2022, with both maximum and mean value decreasing, data for 2023 report a new increase with the annual average growing to the value of 0.0434 mol/m^2.

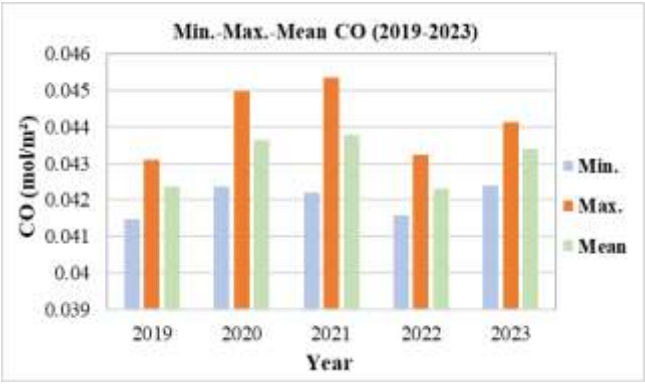
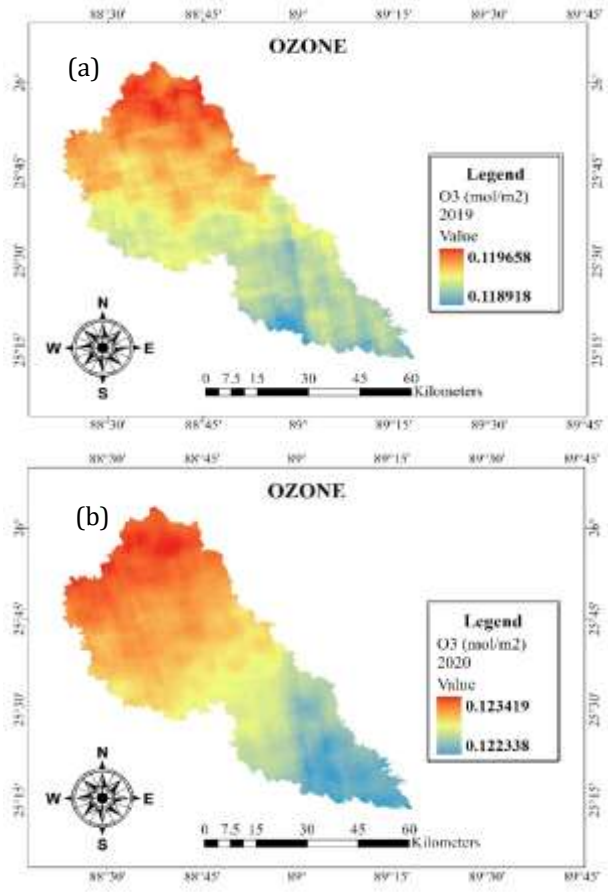


Figure 11. Min-max-mean CO chart (2019-2023)

3.4. Variation of O_3

The O_3 spatial pattern is presented in Figures 12(a-e) particularly high in northern part of Dinajpur. Ozone is produced in a highly dependent manner on daylight, and temperature; showing marked seasonal maxima. Monthly mean ozone (O_3) profile for Dinajpur (2019–2023), which reflects a well-defined solar-driven seasonal cycle reaching its maximum value in the high-insolation pre-monsoon season, are shown in Figures 13(a-e). In contrast to the primary pollutants, O_3 levels continue accumulating between April and June with annual peak values ranging from 0.127 mol/m^2 (2019) to 0.133 mol/m^2 (2020). They are generally lowest during the lower-light winter or post-monsoon season (0.110–0.115 mol/m^2). Significantly, whereas 2020 and 2023 had pronounced spring peaks, 2022 displayed a persistent five-month period of high ambient ozone levels.



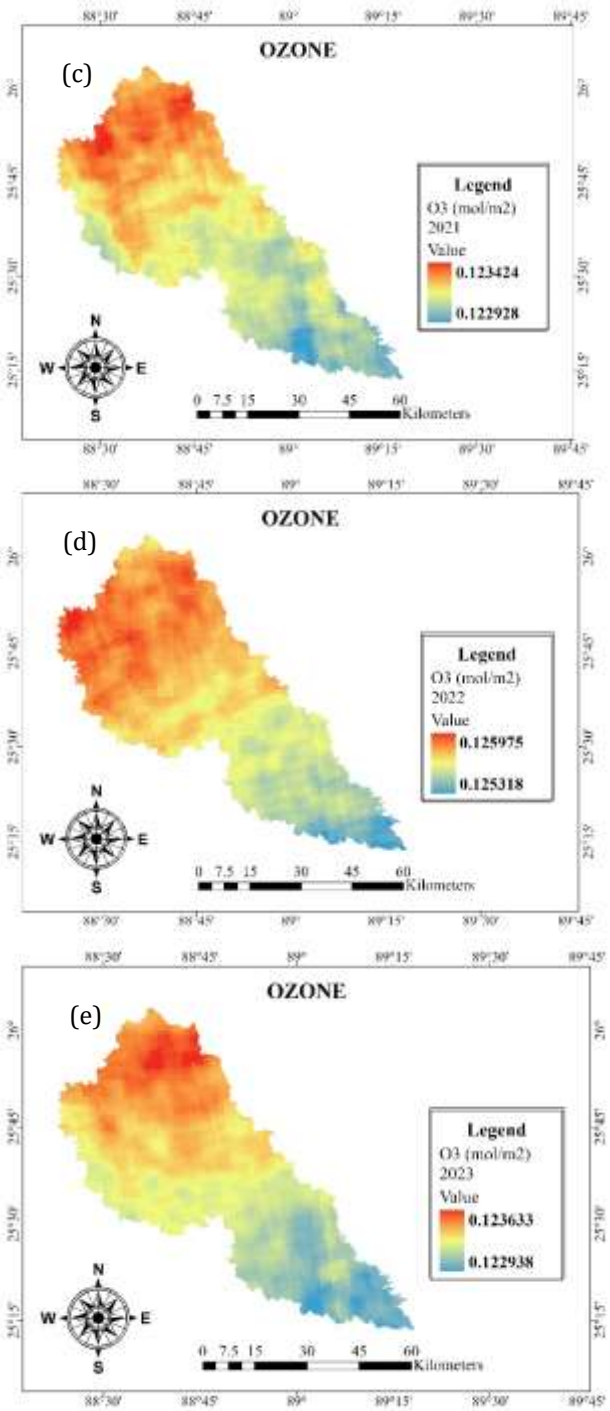
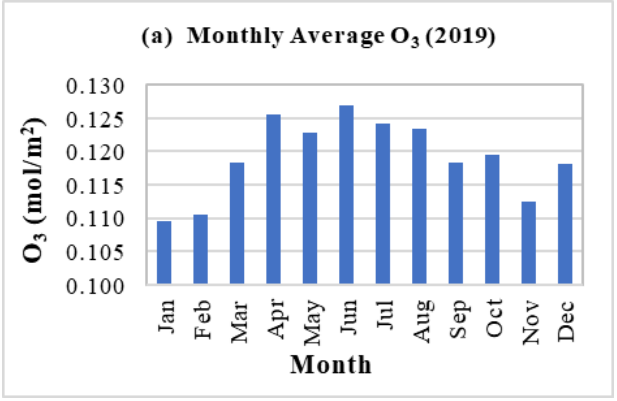
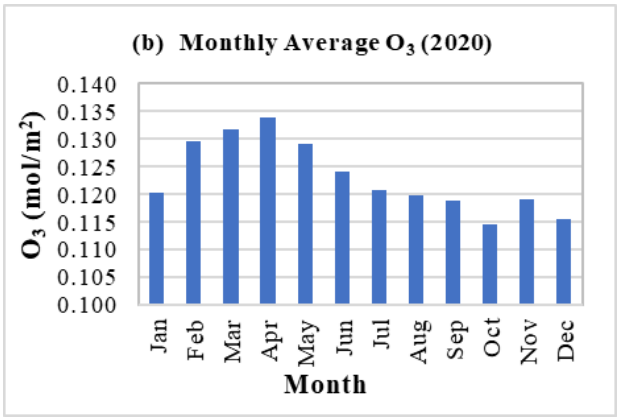
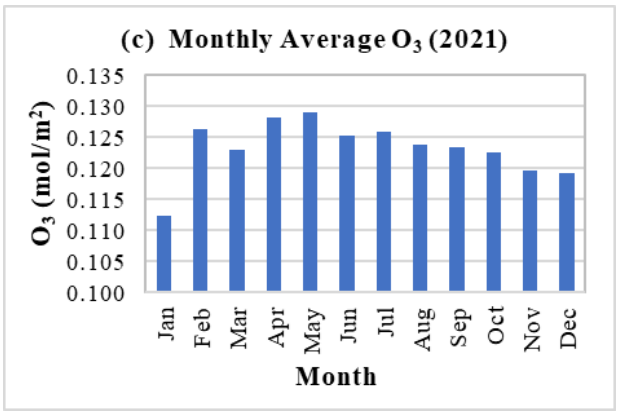
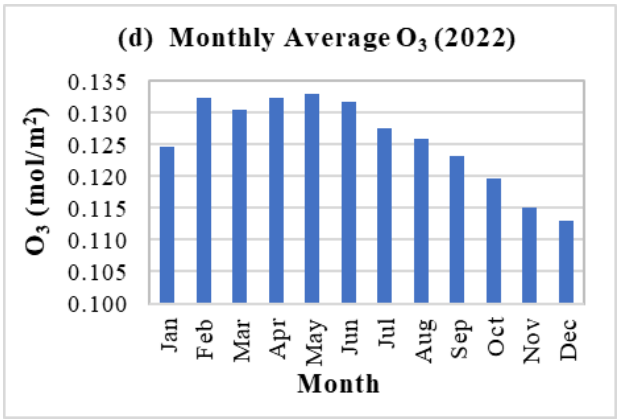


Figure 12. Spatial maps of O_3 for (a) 2019 (b) 2020 (c) 2021 (d) 2022 (e) 2023









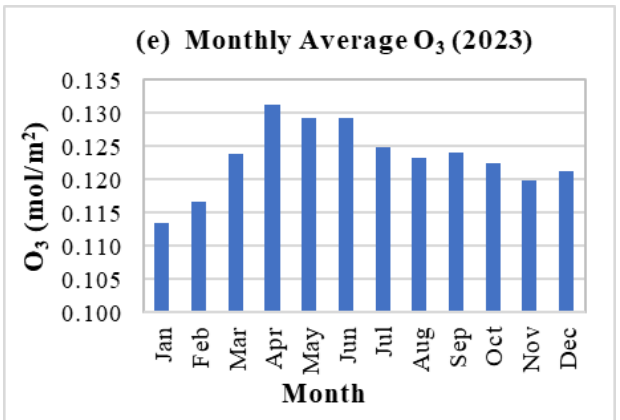


Figure 13. Monthly average values of O_3 for (a) 2019 (b) 2020 (c) 2021 (d) 2022 (e) 2023

Figure 14 clearly indicates that the annual statistical profile of ozone in Dinajpur (2019–2023) started to accumulate from 2019 towards its highest level in 2022 and then decline. All three important values (minimum,

maximum and mean) all rose after each had been recorded at its lowest measurement in 2019 (mean ≈ 0.119 mol/m^2), to set the dataset maximum where mean was around 0.126 mol/m^2 in this 2022 comparison year. This upward trend shows a steady increase of ozone pollution in the four years overall. In 2023, however, the annual mean broke this trend and reduced to ~0.123 mol/m^2, indicating possible stabilization or decrease in photochemical activity post-peak year.

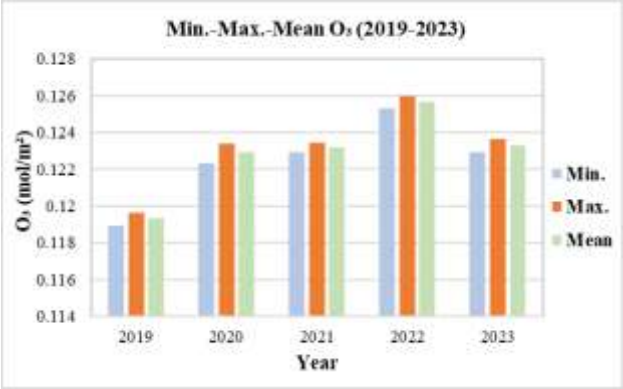
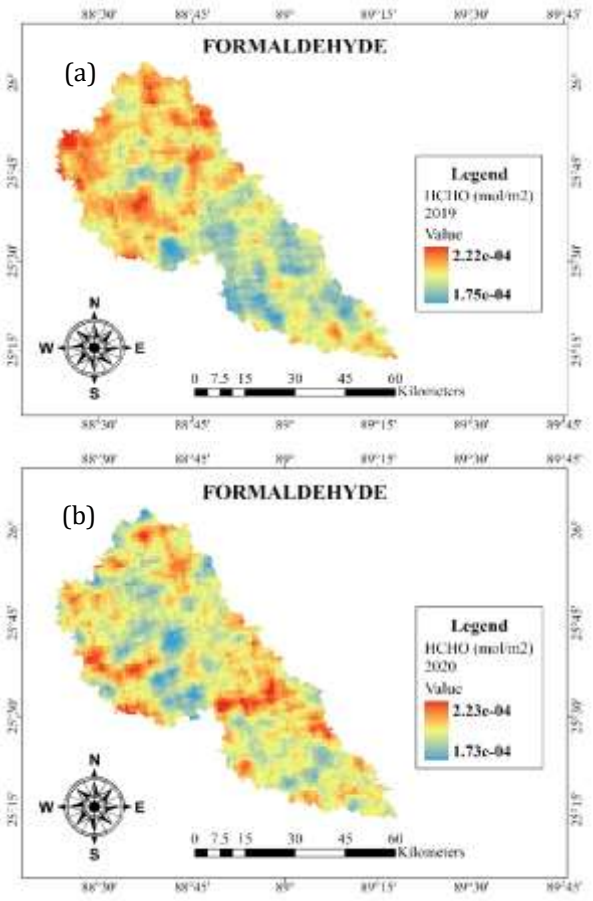


Figure 14. Min-max-mean O3 chart (2019-2023)

3.5. Variation of HCHO

The tropospheric column density maps of HCHO represented in Figures 15(a-e) reveal increased values at agricultural belts and peri-urban areas of Bochaganj, Dinajpur Sadar, and Parbatipur. There are both direct emissions sources (vehicles, brick kilns) and secondary generation from lower VOCs (Volatile Organic Compounds).



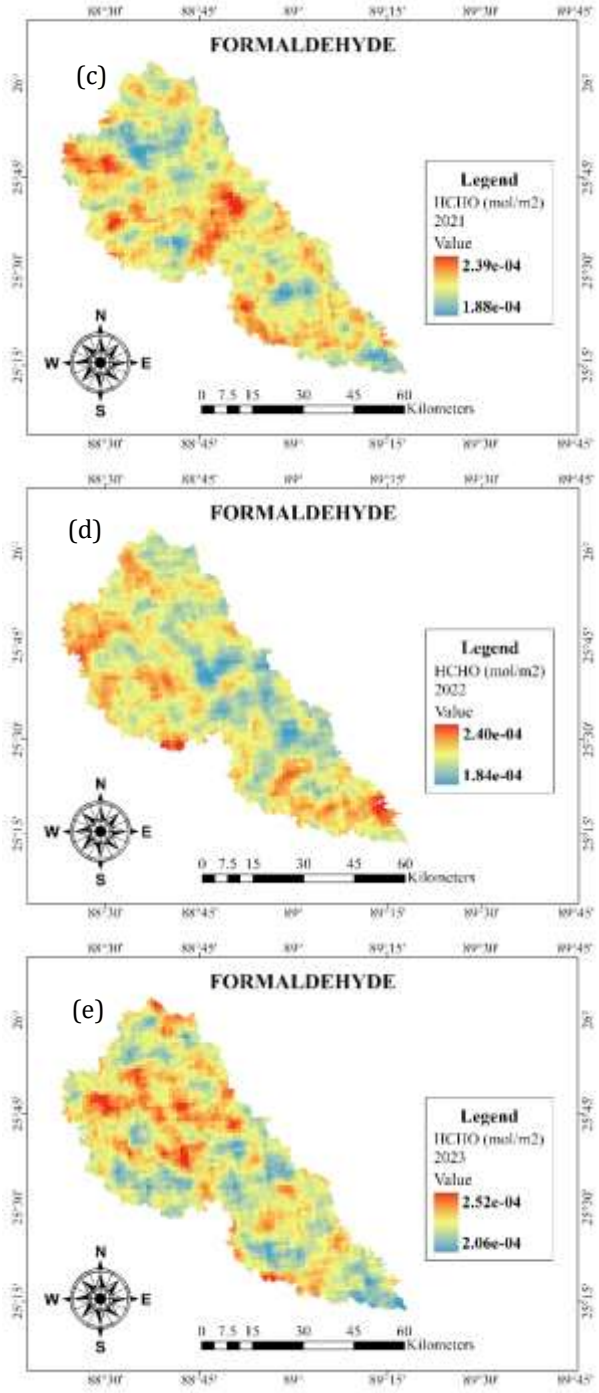


Figure 15. Spatial maps of HCHO for (a) 2019 (b) 2020 (c) 2021 (d) 2022 (e) 2023

The seasonality of HCHO in Dinajpur (2019–2023) is mainly influenced by HCHO during the pre-monsoon and summer periods as observed from their temporal variability (Figures 16a-e). Compared with primary pollutants, which are dominated in winter season, HCHO column densities usually rises up to the maximum level during the period from April to June associated with high temperature and solar radiation.

For example, May 2019 (0.00023 mol/m^2), April 2021 (0.00027 mol/m^2) and June 2023 (0.00028 mol/m^2) had individual peaks. This indicates that the HCHO in this region is strongly affected by secondary photochemical production and temperature-induced biogenic emission. But meteorological variation

particularly changed this pattern in 2020 and 2022, with the higher levels continuing or peaking in winter (December), suggesting that under some circumstances anthropogenic or atmospheric stagnation are also responsible for HCHO buildup. The 5-year time series trend of Formaldehyde (HCHO) in Dinajpur (2019–2023) (Figure 17), an increase for all the statistical parameters is observed consistently. The annual mean column densities increased from a minimum value of 0.00019 mol/m^2 in 2019 to a maximum of 0.00023 mol/m^2 in 2023.

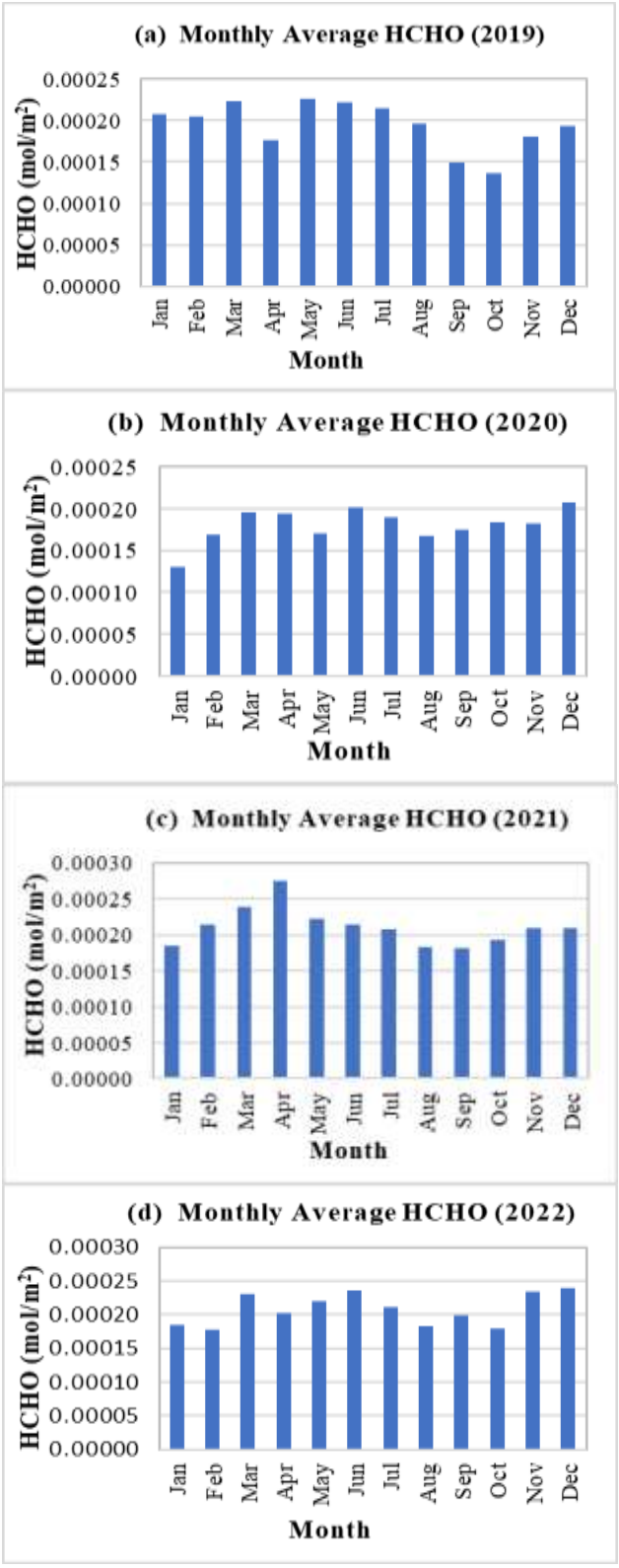




Figure 16. Monthly average values of HCHO for (a) 2019 (b) 2020 (c) 2021 (d) 2022 (e) 2023

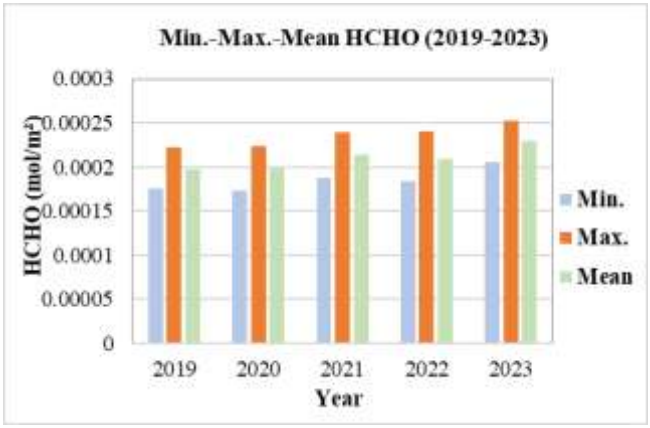


Figure 17. Min-max-mean HCHO chart (2019-2023)

This increase is the result of both an increasing pollution ceiling reaching more than 0.00025 mol/m^2 by 2023 and a rising floor, with minimum column densities of more than 0.00020 mol/m^2 that increased over the monitoring period compared to those above as measured in approximately 0.000175 mol/m^2 throughout the study time-span. Although there are no specified ground-based monitoring stations for gaseous pollutants in Dinajpur, a commentator on the adverse pollution phenomena exhibited by our Sentinel-5P TROPOMI data is in fact the drastic air quality degradation reported recently and everywhere else in the northern and northwestern cities. Importantly, unlike our study, which relies on satellite and ground-based air quality assessments, previous studies into the air quality in this northern region, including Dinajpur, Rangpur, and Rajshahi have only used localized ground-level concentration measurements, focusing mainly on particulate matter ($PM_{2.5}$ and PM_{10}). To the best of our knowledge, this is the first study using satellite-derived tropospheric column densities to investigate the spatiotemporal variations in trace gaseous pollutants across these cities. For example, $PM_{2.5}$ and PM_{10} were 56.41 μg/m^3 and 72.63 μg/m^3 at the same location, exceeding WHO (World Health Organization) standards up to 2.25 times for $PM_{2.5}$ and 1.45 times for PM_{10} [57]. This was also the case for the Rangpur metropolitan area, which has critically high average ground-level concentrations of $PM_{2.5}$ (70.13 μg/m^3) and PM_{10} (89.66 μg/m^3). While mainly concerned with particulate matter, checks carried out in research hubs bolstered these observations by demonstrating significant sectoral

neglect amid common anthropogenic factors that drive widespread regional pollution across the greater North of Bangladesh: uncontrolled vehicle emissions, accelerating commercial urbanization, and operation of brick kilns near densely populated areas [57-58]. Moreover, regional atmospheric modeling and spatial analyses have shown that local air pollution has been substantially increased by the effects of regional transport and transboundary air pollution [59]. Since industrialization is highly concentrated in some areas, such as the eastern Parbatipur upazila [58], heavy industrial activities like coal mining and coal-based power generation dominate pollution sources. During the dry season, average wind currents are east (Parbatipur) toward west (Dinajpur Sadar), with mean velocity values reaching 3 m/s and leading to regional flows that serve as transport phenomena throughout the area [60]. In fact, this meteorological parameter plays an active role in transporting massive amounts of industrial pollutants, such as the precursors for NO_2 and SO_2 to secondary pollutants like O_3, into the core Dinajpur hotspots. As a result, the significant pollutant column densities in Dinajpur Sadar are not merely due to localized urban emissions but are significantly aggravated by regional transport of plumes from eastern industrial sectors and transboundary sources [59].

3.6. Air pollution risk zone mapping

The combined air pollution risk image (Figure 18) presents an integrated view of the cumulative exposure to NO_2, SO_2 CO, O_3 and HCHO in Dinajpur district. The risk surface estimated using normalized multi-criteria overlay technique exhibits spatial clustering of high-risk areas. The central-western regions are the most dangerous area and have a dense red cluster (high risk) representing the combined effect of NO_2, SO_2, CO, O_3 and HCHO.

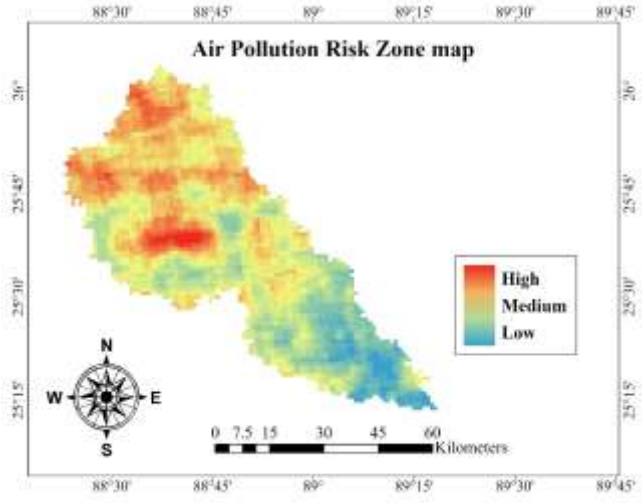


Figure 18. Air pollution risk zone map

The location is situated to the west and south-west of Dinajpur Sadar and characterized by high density of brick kilns, heavy traffic related activities and increasing populations, which lead to heavy emissions throughout the year. Moderate-risk areas are spread over the north-western and mid-central region, where semi-urban activity and agriculture burning add to intermittent pollution. On the other hand, in a large part of the south-eastern and eastern regions there are only low risks (blue) that can be attributed to low population density, more vegetation coverage or fewer industrial sources. Geographical distribution is consistent with individual pollutant maps, indicating that emission sources are highly aggregated in the west of the district. Such risk assessment would be very useful, particularly in Dinajpur, where there are no ground monitoring stations and help address priority areas for emission reduction and environmental management (Table 1).

Table 1. Risk category thresholds

AQRI	Risk
0-0.26	Low
0.26-0.41	Moderate
0.41-0.72	High

Despite being fundamentally different from a typical air quality index such as the air quality index (AQI) or even the air quality health index (AQHI), spatial patterns identified in this study are consistent with pollution-prone zones previously reported in northern Bangladesh. In contrast to AQI, which reflects ground-level concentrations and health thresholds at these sites, the aerosol quality risk index links satellite-derived column densities to a spatially relative risk assessment for the regions lacking monitoring stations. While alternative weighting schemes may affect AQRI magnitude, they would likely not change the pattern of spatial hotspots because normalization adjusts pollutant variability. The AQRI developed in this study provides relative spatial differences in atmospheric pollutant exposure rather than absolute health risk. Given that Sentinel-5P measures column densities rather than surface concentrations, AQRI outputs should be interpreted as Phyto toxicological risk coefficients and not regulatory air quality grades.

3.7. Statistical trend analysis

Statistically significant increasing trends for NO_2 and HCHO column densities over the Dinajpur District were detected during 2019–2023 according to the Mann–Kendall trend test ($p < 0.05$) (Table 2). For NO_2, there was a positive trend ($\tau = 0.218$, $p = 0.014$) with a Sen's slope of 2.01×10^{-7} mol m^{-2} per month, corresponding to an overall increase of 10.58%. HCHO demonstrated the highest increase over time ($\tau = 0.244$, $p = 0.006$), with an average increase of 18.09% during the review timeframe too. Conversely, SO_2, O_3, and CO did not demonstrate statistically significant trends ($p > 0.05$), with column density variations remaining comparatively stable despite minor fluctuations highlighted in plots of temporal data. These observations indicate that visual interpretation alone can exaggerate perceived trends that are not statistically verified. All pollutants showed similar trends over time as illustrated in Figure 19.

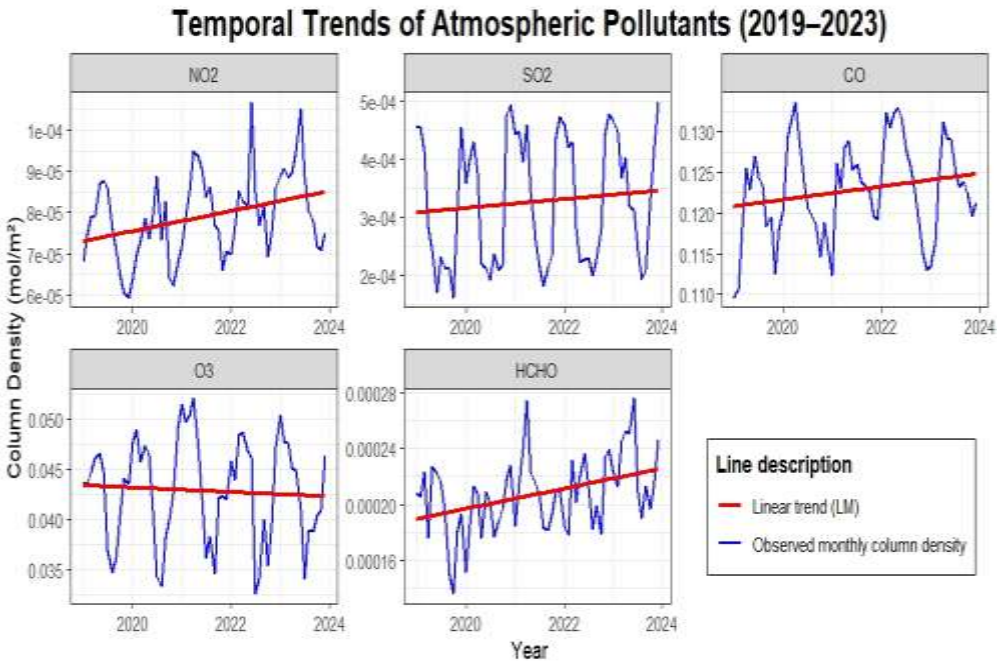


Figure 19. Temporal trends of pollutants

Atmospheric pollutant correlations were analyzed using Pearson correlation analysis (Figure 20). The correlation was strongly positive between the NO_2 and HCHO (r = 0.62), hinting at possible relations of nitrogen oxide emissions with photochemical production of formaldehyde in the atmosphere. Similarly, SO_2 also correlated positively and strongly with O_3 (r = 0.62), potentially reflecting co-occurring atmospheric processes tied to oxidation and regional atmospheric chemistry. A moderate correlation was found between NO_2 and CO (r=0.47) suggesting possible influence from common emission sources related to combustion such as transport and fuel burning. HCHO also showed weak to moderate positive correlations with SO_2 (r = 0.38) and O_3 (r = 0.36). On the contrary, low negative correlations between SO_2 and CO (r = −0.27) as well as NO_2 and SO_2 (r = −0.20) were found implying that these substances arise from partially distinct emission processes or diversity of atmospheric behavior.

Table 2. Statistical trends

Pollutant	MK_Tau	p_value	Sen_slope	Percent_change	Trend
NO2	0.218	0.014	0.000000201	10.58%	Increasing
SO2	0.064	0.471	0.000000444	9.46%	No significant trend
O3	-0.036	0.688	-0.0000207	5.98%	No significant trend
CO	0.11	0.218	0.0000529	10.61%	No significant trend
HCHO	0.244	0.006	0.000000527	18.09%	Increasing

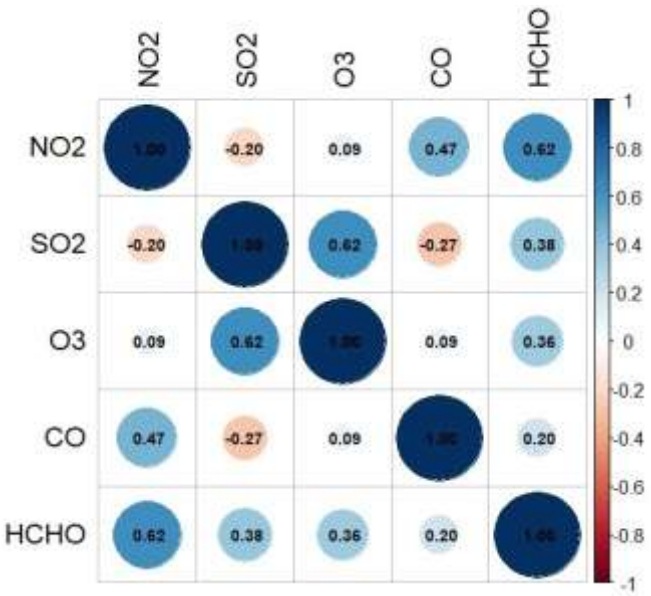


Figure 20. Correlation matrix visualization

In summary, correlation patterns reveal the intricate interactions between atmospheric pollutants and how not only emission sources but also atmospheric chemistry contribute to their temporal variability. During 2020, a prominent decrease in pollutant column densities has been reported across South Asia coinciding with COVID-19 lockdown restrictions [61]. Regional studies have also showed similar reductions in NO_2 and CO concentrations during lockdowns, as vehicle transportation and industrial activities decreased (Figure 21). The reported temporary decline in this study, therefore, seems more associated with reduced anthropogenic events rather than an improvement of our atmosphere on a long-term scale. The results are based on satellite-derived column densities and not concentrations at the ground level; as a result, observed COVID-19 impacts indicate atmospheric column responses and not direct exposure changes during the COVID time period.

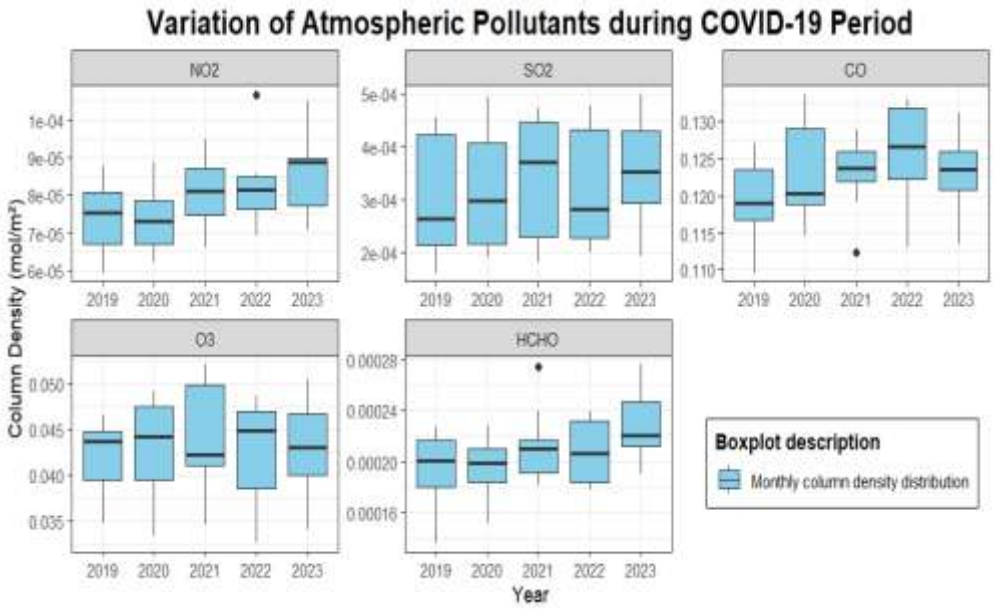


Figure 21. Inter-annual variation of atmospheric pollutants

3.8. Mechanistic understanding and driving factors

Regional emission sources and meteorological controls explain part of the observed spatial and temporal variability of atmospheric pollutants. Stationary source emissions are primarily concentrated around deposition sites due to high urbanization along access routes, which was consistent with the reported emission sources in northern Bangladesh for vehicular, brick kiln, and fossil-fuel combustion activities. Brick kilns and transportation emissions are already known to play a major role in nitrogen oxide and sulfur dioxide levels in South Asian cities. Meteorological conditions highly impactful seasonal variability of pollutants concentration during the winter months, low boundary layer heights and light winds restrict dispersion capacity in the atmosphere, leading to pollutant accumulation. On the other hand, the monsoon precipitation contributes to increasing wet deposition of pollutants and atmospheric cleaning, thus resulting in low concentrations of pollutants. Temperature and solar radiation also affect atmospheric chemistry by increasing photochemical processes.

Primary pollutants (NO_2, SO_2, and CO) are derived not only from direct emissions but also from secondary pollutants (O_3 and HCHO), whose relationship reflects the photochemical oxidation processes. Tropospheric ozone (O_3) forms in the presence of sunlight through reactions between nitrogen oxides and volatile organic compounds, whereas formaldehyde (HCHO) is a marker for VOC oxidation and secondary photochemistry. Higher levels of solar radiation in the pre-monsoon period may further magnify these reactions, elucidating the seasonal trends observed for secondary species. Moreover, air masses moving from industrial regions in neighboring South Asia can affect the regional transboundary transport of pollutants and impact pollutant levels in Bangladesh. On a larger scale, long-range transport has been highlighted as an important contributor to the pervasively high pollution levels at background sites throughout the Indo-Gangetic plain and it substantially affects local air quality depending on local emission sources.

3.9. Policy implications and recommendations

The results offer important implications for air-quality management and environmental policy. A range of pollution hotspots was identified through satellite-derived spatial risk maps, indicating urgency and priority for mitigation in traffic-emissions-impacted areas, industrial activities, brick kilns, and urban construction. The emission control measures, such as stringent standards for emissions, use of cleaner fuels and improved traffic management, should be targeted in these microenvironments to proactively minimize pollutant concentrations that have high health risk. Satellite observations, for example from Sentinel-5P, provide an effective means of monitoring large-scale atmospheric pollution patterns and spotting emerging hotspots. Combining satellite data with national monitoring programs under the auspices of the Department of Environment and increasing ground-based monitoring networks can improve validation, strengthen environmental surveillance, and provide evidence-based air-quality management policies.

3.10. Study limitations

While this study discovered spatial pollution patterns based on observations from satellite imagery identifying the nature of individual emission sources (for example, brick kilns versus traffic density), a detailed analysis using such local emission inventories was not possible in the current research as high-resolution emission datasets were limited. Further studies with emission inventories and land-use data will allow for quantitative source attribution. Meteorological drivers like wind speed, boundary layer height, and temperature variability were discussed qualitatively but not quantitatively in statistical modeling. Over more extended periods, the inclusion of reanalysis

meteorological datasets (e.g., ERA5) could assist with mechanistic interpretation of seasonal variability. Moreover, we inferred transboundary pollution transport from regional atmospheric behavior as discussed in previous studies, instead of trajectory modeling methods such as HYSPLIT. Future investigations should leverage air-mass trajectory analysis to quantitatively assess their regional transport contributions. Consequently, the AQRI developed in this study reflects relative spatial risk patterns but not absolute causal attribution of pollution sources.

4. Conclusion

This research employed a five-year record of Sentinel-5P TROPOMI data (2019–2023) to carry out the first-ever survey covering both spatial and temporal dimensions on atmospheric pollution in Dinajpur District. The study has quantified the accumulation of NO_2, SO_2, CO, O_3 and HCHO over a rapidly developing region where ground-based air quality monitoring infrastructure is not available by combining cloud-based processing on Google Earth Engine and multi-criteria GIS analysis. The statistical analysis with annual mean column densities shows a clear worrying tendency in atmospheric deterioration for the period observed. The four other pollutants all trended upwards during the period, with CO having a spike in 2021 before steadying. NO_2 and SO_2 levels have consistently increased, with both annual averages exceeding the peaks of 2019 for the observation period ranging from 2020 to 2023. Also, Formaldehyde (HCHO) exhibits a clear increase in the data, and we conclude that both biogenic and anthropogenic hydrocarbon emissions are rising. O_3 (a secondary pollutant) showed a continuous accumulation maximum in 2022, indicating the growing capacity for photochemical smog formation of this area. Taken together, the trends clearly demonstrate that the atmospheric load-bearing capacity of Dinajpur is being increasingly threatened by intensifying anthropogenic practices. Individual pollutants did not have a uniform spatial distribution but instead exhibited hotspots and localized areas affected by land use. NO_2 and SO_2 were severely accumulated in the central zone of governmental activities, typical industrial site areas in the district, which is positively related to the density of brick kilns and vehicular road network. In contrast, the more spatially extensive impacts due to pollutants such as HCHO and SO_2 reflect their secondary formation processes in peri-urban and agricultural regions. The Air Pollution Risk Map combined these disparate spatial patterns into a single index and revealed a chasm in environmental vulnerability throughout the district:

- ✓ High-Risk Core (Central zone): The cumulated exposure pollution risk is absolutely concentrated in Dinajpur Sadar. This core of the island constitutes a high-risk island (area shown as deep red in risk maps) where peak levels of several pollutants overlap. This is an indication that the district headquarters was both the origin and target of accumulated atmospheric load.
- ✓ Moderate-Risk Spreading Area (NorthWest & East Belts): The risk of pollution is transmitted from the central area to other areas. Moderate risk areas (yellow/orange) can also be seen to the North (Birganj and Kaharole), West (Biral), as well as to the East (Parbatipur). This suggests a corridor of deteriorating air quality most probably due to transportation corridors and the growing semi-urban settlements that connect these upazilas with the centre.
- ✓ Low-Risk Havens (SouthEastern Zone): There is a pronounced trend of decreased risk going southeast. The upazilas of Nawabganj, Hakimpur, and Ghoraghat tend to show the lowest risk index (blue zones) that may be attributed to lower industrial density and greater distance from the central urban agglomeration.

The results indicate that air pollution has become a district-level problem in Dinajpur with particular Central-western axis threshold of vulnerability. Recognition of Dinajpur Sadar as an important multi-pollutant hotspot emphasizes the necessity for focused intervention in this area. This study generates scientific evidence that can be used by policymakers to rank emission control in the identified high-risk upazilas and help prevent further exposure from urbanization at the expense of environmental health of the area.

Acknowledgement

The authors are very grateful to all individuals associated with this study who have contributed to its completion.

Author contributions

Md. Mahfuj Ahmed Sizan: Conceptualization, Data Collection, Methodology, Software, Writing-Original draft preparation **Md. Mahabub Rahman:** Methodology, Software, Writing-Original draft preparation, Reviewing and Editing **Md. Osman Gani Rasel:** Data curation, Software, Writing-Writing-Reviewing and Editing **Mehedy Sultan Sohan:** Visualization, Investigation, Writing-Reviewing and Editing **Pallab Nag:** Visualization, Investigation, Writing-Reviewing and Editing.

Conflicts of interest

The authors declare no conflicts of interest.

References

1. Brauer, M., Freedman, G., Frostad, J., Van Donkelaar, A., Martin, R. V., Dentener, F., ... & Cohen, A. (2016). Ambient air pollution exposure estimation for the global burden of disease 2013. *Environmental science & technology*, *50*(1), 79-88. https://doi.org/10.1021/acs.est.5b03709
2. Chen, T. M., Kuschner, W. G., Gokhale, J., & Shofer, S. (2007). Outdoor air pollution: ozone health effects. The American journal of the medical sciences, 333(4), 244-248.

https://doi.org/10.1097/MAJ.0b013e31803b8e8c
3. Chow, J. C., Watson, J. G., Mauderly, J. L., Costa, D. L., Wyzga, R. E., Vedal, S., ... & Dockery, D. W. (2006). Health effects of fine particulate air pollution: lines that connect. Journal of the air & waste management association, 56(10), 1368-1380. https://doi.org/10.1080/10473289.2006.10464545
4. WHO. (2021). Air quality database 2021. World Health Organization.
5. Monks, P. S., Archibald, A. T., Colette, A., Cooper, O., Coyle, M., Derwent, R., ... & Williams, M. L. (2015). Tropospheric ozone and its precursors from the urban to the global scale from air quality to short-lived climate forcer. *Atmospheric chemistry and physics*, *15*(15), 8889-8973. https://doi.org/10.5194/acp-15-8889-2015
6. Khan, R., Kumar, K. R., & Zhao, T. (2021). Assessment of variations of air pollutant concentrations during the COVID-19 lockdown and impact on urban air quality in South Asia. Urban climate, 38, 100908. https://doi.org/10.1016/j.uclim.2021.100908
7. Pavel, M. R. S., Zaman, S. U., Jeba, F., Islam, M. S., & Salam, A. (2021). Long-term (2003–2019) air quality, climate variables, and human health consequences in Dhaka, Bangladesh. Frontiers in Sustainable Cities, 3, 681759. https://doi.org/10.3389/frsc.2021.681759
8. Marlier, M. E., Jina, A. S., Kinney, P. L., & DeFries, R. S. (2016). Extreme air pollution in global megacities. Current Climate Change Reports, 2(1), 15-27. https://doi.org/10.1007/s40641-016-0032-z
9. Rahman, M. M., Hasanuzzaman, A. B. M., Chisty, M. A., Alam, E., Islam, M. K., & Islam, A. R. M. T. (2025). Perceived-air pollution and self-reported health status: a study on air pollution-prone urban area of Bangladesh. Frontiers in Public Health, 13, 1382471. https://doi.org/10.3389/fpubh.2025.1382471
10. Hoque, M. M. M., Mizan, M. M. R., Hossain, M. N., Sarker, M. E., Pranto, N. N., Khan, M. M. H., ... & Yesmin, R. (2025). Spatial distribution and diurnal variation of particulate matters and gaseous air pollutants of Dhaka city, Bangladesh. *Discover Atmosphere*, *3*(1), 10.
11. Huraira, A., Jui, T. J., Samm, A., Samad, N., & Sarker, S. (2024). Spatial Trend Analysis of Atmospheric Pollutants in Chattogram District of Bangladesh using Sentinel-5 TROPOMI Images. The Dhaka University Journal of Earth and Environmental Sciences, 13(2), 105-123. https://doi.org/10.3329/dujees.v13i2.79465
12. Mahmud, H., Shobnom, K., Ali, M. R., Muntakim, N., Kulsum, U., Baroi, D. S., ... & Hassan, M. Z. (2024). Micro-environmental dynamics of particulate ($PM_{2.5}$ and PM_{10}) air pollution in Rajshahi City: a spatiotemporal analysis. Management of Environmental Quality: An International Journal, 35(8), 1773-1797. https://doi.org/10.1108/MEQ-08-2023-0265
13. Mukta, T. A., Hoque, M. M. M., Sarker, M. E., Hossain, M. N., & Biswas, G. K. (2020). Seasonal variations of gaseous air pollutants (SO_2, NO_2, O_3, CO) and particulates ($PM_{2.5}$ and PM_{10}) in Gazipur: an industrial city in Bangladesh. *Advances in Environmental Technology*, *6*(4), 195-209. https://doi.org/10.22104/aet.2021.4890.1320
14. Saha, M. K., Ahmed, S. J., Sheikh, A. H., & Mostafa, M. G. (2021). Impacts of Brick Kilns on Environment around Kiln areas of Bangladesh. Jordan Journal of Earth & Environmental Sciences, 12(3).
15. Guttikunda, S. K., Begum, B. A., & Wadud, Z. (2013). Particulate pollution from brick kiln clusters in the Greater Dhaka region, Bangladesh. Air Quality, Atmosphere & Health, 6(2), 357-365. https://doi.org/10.1007/s11869-012-0187-2
16. Begum, B. A., & Hopke, P. K. (2018). Ambient air quality in Dhaka Bangladesh over two decades: Impacts of policy on air quality. Aerosol and Air Quality Research, 18(7), 1910-1920. https://doi.org/10.4209/aaqr.2017.11.0465
17. Dhankar, S., & Pani, B. (2025). Spatio-temporal analysis of formaldehyde and its association with atmospheric and environmental variables over the Southeast Asian region using satellite data. Environmental Monitoring and Assessment, 197(2), 185. https://doi.org/10.1007/s10661-025-13617-2
18. Ma, W., Feng, Z., Zhan, J., Liu, Y., Liu, P., Liu, C., ... & Liu, J. (2022). Influence of photochemical loss of volatile organic compounds on understanding ozone formation mechanism. Atmospheric Chemistry and Physics, 22(7), 4841-4851. https://doi.org/10.5194/acp-22-4841-2022
19. Pinto, D. M., Blande, J. D., Souza, S. R., Nerg, A. M., & Holopainen, J. K. (2010). Plant volatile organic compounds (VOCs) in ozone (O3) polluted atmospheres: the ecological effects. Journal of chemical ecology, 36(1), 22-34. https://doi.org/10.1007/s10886-009-9732-3
20. Srivastava, A., Thakur, A. K., & Garg, R. D. (2025). An assessment of the spatiotemporal dynamics and seasonal trends in NO_2 concentrations across India using advanced statistical analysis. Remote Sensing Applications: Society and Environment, 37, 101490. https://doi.org/10.1016/j.rsase.2025.101490
21. Amani, M., Ghorbanian, A., Ahmadi, S. A., Kakooei, M., Moghimi, A., Mirmazloumi, S. M., ... & Brisco, B. (2020). Google earth engine cloud computing platform for remote sensing big data applications: A comprehensive review. *IEEE Journal of Selected Topics in Applied Earth Observations and Remote Sensing*, *13*, 5326-5350.

https://doi.org/10.1109/JSTARS.2020.3021052

22. Veefkind, J. P., Aben, I., McMullan, K., Förster, H., De Vries, J., Otter, G., ... & Levelt, P. F. (2012). TROPOMI on the ESA Sentinel-5 Precursor: A GMES mission for global observations of the atmospheric composition for climate, air quality and ozone layer applications. Remote sensing of environment, 120, 70-83. https://doi.org/10.1016/j.rse.2011.09.027
23. Zhao, X., Griffin, D., Fioletov, V., McLinden, C., Cede, A., Tiefengraber, M., ... & Lee, S. C. (2020). Assessment of the quality of TROPOMI high-spatial-resolution NO_2 data products in the Greater Toronto Area. Atmospheric Measurement Techniques, 13(4), 2131-2159. https://doi.org/10.5194/amt-13-2131-2020
24. Mohamed, H., Hassan, A., & Elhag, A. (2025). A five-year Study Using Sentinel-5P Data Observing Seasonal Dynamics and Long-term Trends of Atmospheric Pollutants. International Journal of Engineering and Geosciences, 10(2), 262-271. https://doi.org/10.26833/ijeg.1587122
25. Kaplan, G., & Avdan, Z. Y. (2020). Space-borne air pollution observation from sentinel-5p tropomi: Relationship between pollutants, geographical and demographic data. International Journal of Engineering and Geosciences, 5(3), 130-137. https://doi.org/10.26833/ijeg.644089
26. Mogaraju, J. K. (2024). Machine learning assisted prediction of land surface temperature (LST) based on major air pollutants over the Annamayya District of India. International Journal of Engineering and Geosciences, 9(2), 233-246. https://doi.org/10.26833/ijeg.1394111
27. Bechle, M. J., Millet, D. B., & Marshall, J. D. (2013). Remote sensing of exposure to NO2: Satellite versus ground-based measurement in a large urban area. Atmospheric Environment, 69, 345-353. https://doi.org/10.1016/j.atmosenv.2012.11.046
28. Theys, N., Hedelt, P., De Smedt, I., Lerot, C., Yu, H., Vlietinck, J., ... & Van Roozendael, M. (2019). Global monitoring of volcanic SO2 degassing with unprecedented resolution from TROPOMI onboard Sentinel-5 Precursor. Scientific reports, 9(1), 2643. https://doi.org/10.1038/s41598-019-39279-y
29. Kotan, B., & Erener, A. (2022). Seasonal analysis and mapping of air pollution (PM10 and SO2) during Covid-19 lockdown in Kocaeli (Türkiye). International Journal of Engineering and Geosciences, 8(2), 173-187. https://doi.org/10.26833/ijeg.1111699
30. Bak, J., Liu, X., Abad, G. G., & Yang, K. (2025). An extension of ozone profile retrievals from TROPOMI based on the SAO2024 algorithm. Remote Sensing, 17(5), 779. https://doi.org/10.3390/rs17050779
31. Kwiecień, J., & Szopińska, K. (2020). Mapping carbon monoxide pollution of residential areas in a Polish city. Remote Sensing, 12(18), 2885. https://doi.org/10.3390/rs12182885
32. Jumaah, H., Kamran, K. V., Ghanbari, A., & Jeihouni, M. (2026). Development of GIS-based box model tool for air quality mapping with Python and ArcGIS Pro in Kirkuk City, Iraq. International Journal of Engineering and Geosciences, 11(1), 212-225. https://doi.org/10.26833/ijeg.1710723
33. De Smedt, I., Pinardi, G., Vigouroux, C., Compernolle, S., Bais, A., Benavent, N., ... & Van Roozendael, M. (2021). Comparative assessment of TROPOMI and OMI formaldehyde observations and validation against MAX-DOAS network column measurements. Atmospheric Chemistry and Physics, 21(16), 12561-12593. https://doi.org/10.5194/acp-21-12561-2021
34. Tripathy, P., Agrawal, A., & Koul, S. (2026). Cloud-based flood mapping with Sentinel-1 SAR on Google Earth Engine: Insights from the global flood mapper. In Data-Driven Earth Observation for Disaster Management (pp. 609-622). Elsevier. https://doi.org/10.1016/B978-0-443-33803-8.00045-7
35. Kafes Demirci, B., Yılmaz, O. S., & Balık Şanlı, F. (2025). Investigation of Longoz Forests with Remote Sensing Techniques on Google Earth Engine Platform: The Case of İğneada Longoz Forests (2000–2021). International Journal of Engineering and Geosciences, 11(1), 78-88. https://doi.org/10.26833/ijeg.1650786
36. Rahman, M. M., Thakur, S., Ahmed, S. T., & Sayed, A. (2026). Development of Liquefaction Hazard Map for Dinajpur Municipality, Bangladesh. Journal of Civil Engineering, Science and Technology, 17(1), 19-29. https://doi.org/10.33736/jcest.7382.2026
37. Rahman, M. M., Thakur, S., Ahmed, S. T., & Yasmin, R. (2025). GIS-based development of liquefaction hazard and soil distribution maps for Dinajpur Sadar, Bangladesh. International Journal of Engineering and Geosciences, 11(2), 263-273. https://doi.org/10.26833/ijeg.1662672
38. Rahman, M. M., Hossain, M. B., & Roknuzzaman, M. (2023, April). Effect of peak ground acceleration (PGA) on liquefaction behavior of subsoil: A case study of Dinajpur Sadar Upazila, Bangladesh. AIP Conference Proceedings, 2713, 030002. https://doi.org/10.1063/5.0129770
39. Rahman, M. M., & Biswas, M. E. (2026). Machine Learning Algorithm-Based Prediction of Groundwater Table in Bogura District, Bangladesh. Turkish Journal of Engineering, 10(3), 936-947. https://doi.org/10.31127/tuje.1808553
40. Rahman, M. M., Islam, M. T., Roknuzzaman, M., Ansary, S., & Hossain, M. N. (2025). GIS-Based Physiochemical and Regression Analysis of

Drinking Water Quality in Dhaka South City Corporation, Bangladesh. International Journal of Engineering and Geosciences, 11(2), 321-335. https://doi.org/10.26833/ijeg.1705195

41. Rahman, M. M., Sakib, N., Yasmin, R., & Ahmed, R. (2025, December). Assessing Heat Index Changes in the Context of Climate Change in Bangladesh. In Proceedings of International Conference on Civil Engineering Research & Innovations (Vol. 12, p. 14).
42. Rahman, M. M., & Sarder, M. (2026). GIS-based semi-variogram model selection for the preparation of Modified Mercalli Intensity map of Dinajpur Sadar, Bangladesh. International Journal of Engineering and Geosciences, 11(1), 136-148. https://doi.org/10.26833/ijeg.1656666.
43. Hossain, M. B., & Rahman, M. M. (2025). Seismic Microzonation and Probability of Ground Failure Assessment Caused by Liquefaction for Bogura District, Bangladesh. Journal of Rehabilitation in Civil Engineering, 13(2), 218-242. https://doi.org/10.22075/jrce.2024.34111.2086
44. Rahman, M.M., Alam, M.N., & Sarder, M. (2026). GIS-Based Estimation of Corrected Standard Penetration Number Using the Best Semi-Variogram Model for Naogaon Sadar. International Journal of Engineering Technologies IJET, 11(1), 1-16. https://doi.org/10.19072/ijet.1840805
45. Rahman, M. M., Nuhash, M. M. R., & Ray, S. (2025, December). Effect of Land Use/land Cover (LULC) Changes on Land Surface Temperature for Chuadanga, Bangladesh. In Proceedings of International Conference on Civil Engineering Research & Innovations (Vol. 12, p. 14).
46. Rahman, M.M. (2025). GIS based allowable bearing capacity thematic maps of shallow foundation for Bogura District, Bangladesh. International Journal of Engineering and Geosciences, 10(3), 329-338. https://doi.org/10.26833/ijeg.1589939
47. Durap, A. (2025). Beachface steepness modulates erosion but not recovery: multi-decadal spatiotemporal shoreline evidence across 390 transects. Journal of Sea Research, 208, 102644. https://doi.org/10.1016/j.seares.2025.102644
48. Durap, A. (2025). Multi-decadal spatiotemporal shoreline vulnerability assessment (1987–2025): Integrating erosion-accretion dynamics for disaster risk reduction across 90 coastal transects. Natural Hazards, 121(19), 22981–23019. https://doi.org/10.1007/s11069-025-07716-z
49. Lange, K., Richter, A., Schönhardt, A., Meier, A. C., Bösch, T., Seyler, A., ... & Burrows, J. P. (2023). Validation of Sentinel-5P TROPOMI tropospheric NO_2 products by comparison with NO_2 measurements from airborne imaging DOAS, ground-based stationary DOAS, and mobile car DOAS measurements during the S5P-VAL-DE-Ruhr campaign. Atmospheric Measurement Techniques, 16(5), 1357–1389. https://doi.org/10.5194/amt-16-1357-2023
50. Vigouroux, C., Langerock, B., Bauer Aquino, C. A., Blumenstock, T., Cheng, Z., De Mazière, M., ... & Winkler, H. (2020). TROPOMI–Sentinel-5 Precursor formaldehyde validation using an extensive network of ground-based Fourier-transform infrared stations. Atmospheric Measurement Techniques, 13(7), 3751–3767. https://doi.org/10.5194/amt-13-3751-2020
51. Verhoelst, T., Compernolle, S., Pinardi, G., Lambert, J. C., Eskes, H. J., Eichmann, K. U., ... & Zehner, C. (2021). Ground-based validation of the Copernicus Sentinel-5P TROPOMI NO_2 measurements with the NDACC ZSL-DOAS, MAX-DOAS and Pandonia global networks. Atmospheric Measurement Techniques, 14(1), 481–510. https://doi.org/10.5194/amt-14-481-2021
52. Queißer, M., Burton, M., Theys, N., Pardini, F., Salerno, G., Caltabiano, T., Varnam, M., Esse, B., & Kazahaya, R. (2019). TROPOMI enables high resolution SO_2 flux observations from Mt. Etna, Italy, and beyond. Scientific Reports, 9(1), 957. https://doi.org/10.1038/s41598-018-37807-w
53. Martínez-Alonso, S., Deeter, M. N., Baier, B. C., McKain, K., Worden, H., Borsdorff, T., Sweeney, C., & Aben, I. (2022). Evaluation of MOPITT and TROPOMI carbon monoxide retrievals using AirCore in situ vertical profiles. Atmospheric Measurement Techniques, 15(16), 4751–4765. https://doi.org/10.5194/amt-15-4751-2022
54. Sha, M. K., Langerock, B., Blavier, J. F. L., Blumenstock, T., Borsdorff, T., Buschmann, M., ... & Zhou, M. (2021). Validation of methane and carbon monoxide from Sentinel-5 Precursor using TCCON and NDACC-IRWG stations. Atmospheric Measurement Techniques, 14(9), 6249–6304. https://doi.org/10.5194/amt-14-6249-2021
55. Sofieva, V. F., Lee, H. S., Tamminen, J., Lerot, C., Romahn, F., & Loyola, D. G. (2021). A method for random uncertainties validation and probing the natural variability with application to TROPOMI on board Sentinel-5P total ozone measurements. Atmospheric Measurement Techniques, 14(4), 2993–3002. https://doi.org/10.5194/amt-14-2993-2021
56. Keppens, A., Di Pede, S., Hubert, D., Lambert, J. C., Veefkind, P., Sneep, M., ... & Zehner, C. (2024). 5 years of Sentinel-5P TROPOMI operational ozone profiling and geophysical validation using ozonesonde and lidar ground-based networks. Atmospheric Measurement Techniques, 17(13), 3969–3993. https://doi.org/10.5194/amt-17-3969-2024
57. Majumder, A. K., Kamruzzaman, A. M., Rahman, M., & Patoary, M. N. A. (2024). Status of air quality in Rajshahi metropolitan area, Bangladesh. GSC Adv. Res. Rev, 18(1), 201-212.

58. Majumder, A. K., Hossain, M. A., Rahman, M., Patoary, M. N. A., & Islam, M. R. (2025). Spatial Distribution of Air Quality in Rangpur Metropolitan, Bangladesh. International Journal of Atmospheric and Oceanic Sciences, 9(1), 44–57. https://doi.org/10.11648/j.ijaos.20250901.15
59. Majumder, A. K., Mahmud, K. K., Rahman, M., Patoary, Md. N. A., Gautam, S., & Tanima, K. R. (2025). Spatial distribution and health implications of particulate matter concentrations across diverse land use types in Dinajpur District, Bangladesh. Geosystems and Geoenvironment, 4(3), 100397. https://doi.org/10.1016/j.geogeo.2025.100397
60. Ahmed, Md. R., Das, B. K., & Tushar, M. S. H. K. (2023). Investigation of a grid-integrated hybrid energy system for residential and electric vehicle (3-wheeler) loads under schedule grid outage. Alexandria Engineering Journal, 80, 241–258. https://doi.org/10.1016/j.aej.2023.08.057
61. Sharma, S., Zhang, M., Anshika, Gao, J., Zhang, H., & Kota, S. H. (2020). Effect of restricted emissions during COVID-19 on air quality in India. Science of The Total Environment, 728, 138878. https://doi.org/10.1016/j.scitotenv.2020.138878



© Author(s) 2026. This work is distributed under https://creativecommons.org/licenses/by-sa/4.0/